NAVAL POSTGRADUATE SCHOOL
Monterey, California

THESIS

THEORETICAL DEVELOPMENT, DESIGN AND TESTING OF A MAGNETIC FUEL CELL

by

Joseph E. Brennan

December 2002

Thesis Advisor:	Todd Weatherford
Co-Advisor:	Gamani Kurunasiri

Approved for public release; distribution is unlimited

THIS PAGE INTENTIONALLY LEFT BLANK

REPORT DOCUMENTATION PAGE			*Form Approved OMB No. 0704-0188*
Public reporting burden for this collection of information is estimated to average 1 hour per response, including the time for reviewing instruction, searching existing data sources, gathering and maintaining the data needed, and completing and reviewing the collection of information. Send comments regarding this burden estimate or any other aspect of this collection of information, including suggestions for reducing this burden, to Washington headquarters Services, Directorate for Information Operations and Reports, 1215 Jefferson Davis Highway, Suite 1204, Arlington, VA 22202-4302, and to the Office of Management and Budget, Paperwork Reduction Project (0704-0188) Washington DC 20503.			
1. AGENCY USE ONLY *(Leave blank)*	**2. REPORT DATE** December 2002	**3. REPORT TYPE AND DATES COVERED** Master's Thesis	
4. TITLE AND SUBTITLE: Theoretical Development, Design and Testing of a Magnetic Fuel Cell			**5. FUNDING NUMBERS**
6. AUTHOR(S) Brennan, Joseph E.			
7. PERFORMING ORGANIZATION NAME(S) AND ADDRESS(ES) Naval Postgraduate School Monterey, CA 93943-5000			**8. PERFORMING ORGANIZATION REPORT NUMBER**
9. SPONSORING / MONITORING AGENCY NAME(S) AND ADDRESS(ES) N/A			**10. SPONSORING / MONITORING AGENCY REPORT NUMBER**
11. SUPPLEMENTARY NOTES The views expressed in this thesis are those of the author and do not reflect the official policy or position of the Department of Defense or the U.S. Government.			
12a. DISTRIBUTION / AVAILABILITY STATEMENT Approved for public release; distribution is unlimited			**12b. DISTRIBUTION CODE**

13. ABSTRACT *(maximum 200 words)*

A magnetic fuel cell uses high-pressure gas to cause a time-dependant change in magnetic field to generate a voltage based upon Faraday's Induction Law. In this thesis, the use of a compressed magnetic gas passing through a magnetic field is described for generation of electrical power. The first stage of this thesis explores the fundamental physical nature of diamagnetic and paramagnetic gases. Once this stage is completed, it will become clear that there are several methods that can be used to overcome the weak nature of these gasses and achieve useful work, due to pressure-sensitive changes in magnetic susceptibility. The second stage of the thesis develops the theory used to model the operation and physical characteristics of the magnetic fuel cell. The third stage shows the development of the specialized magnetic fields required and equipment configuration necessary to employ the above methods and predicts the experimental measurements of the resulting voltages and currents. The fourth stage discusses experimental findings and presents an optimized configuration. The final stage of the thesis concludes with lessons learned and interesting ramifications of the fuel cell.

14. SUBJECT TERMS Magnetic Fuel Cell, Diamagnetic Gas, Susceptibility, Nitrogen, Magnetic, Permeability, Magnetism, Paramagnetism.			**15. NUMBER OF PAGES** 101
			16. PRICE CODE
17. SECURITY CLASSIFICATION OF REPORT Unclassified	**18. SECURITY CLASSIFICATION OF THIS PAGE** Unclassified	**19. SECURITY CLASSIFICATION OF ABSTRACT** Unclassified	**20. LIMITATION OF ABSTRACT** UL

i

THIS PAGE INTENTIONALLY LEFT BLANK

**THEORETICAL DEVELOPMENT, DESIGN AND TESTING OF A MAGNETIC
FUEL CELL**

Joseph E. Brennan
Lieutenant Commander, United States Navy
B.S., University of Colorado, 1992

Submitted in partial fulfillment of the
requirements for the degree of

MASTER OF SCIENCE IN ELECTRICAL ENGINEERING

from the

**NAVAL POSTGRADUATE SCHOOL
December 2002**

Author: Joseph E. Brennan

Approved by: Todd Weatherford
                        Thesis Advisor

                        Gamani Kurunasiri
                        Thesis Co-Advisor

                        John Powers
                        Chairman
                        Department of Electrical and Computer Engineering

THIS PAGE INTENTIONALLY LEFT BLANK

ABSTRACT

A magnetic fuel cell uses high-pressure gas to cause a time-dependant change in magnetic field to generate a voltage based upon Faraday's Induction Law. In this thesis, the use of a compressed magnetic gas passing through a magnetic field is described for generation of electrical power.

The first stage of this thesis explores the fundamental physical nature of diamagnetic and paramagnetic gases. Once this stage is completed, it will become clear that there are several methods that can be used to overcome the weak nature of these gasses and achieve useful work, due to pressure-sensitive changes in magnetic susceptibility. The second stage of the thesis develops the theory used to model the operation and physical characteristics of the magnetic fuel cell. The third stage shows the development of the specialized magnetic fields required and equipment configuration necessary to employ the above methods and predicts the experimental measurements of the resulting voltages and currents. The fourth stage discusses experimental findings and presents an optimized configuration. The final stage of the thesis concludes with lessons learned and interesting ramifications of the fuel cell.

THIS PAGE INTENTIONALLY LEFT BLANK

TABLE OF CONTENTS

THIS PAGE INTENTIONALLY LEFT BLANK

LIST OF FIGURES

THIS PAGE INTENTIONALLY LEFT BLANK

LIST OF TABLES

THIS PAGE INTENTIONALLY LEFT BLANK

ACKNOWLEDGMENTS

THIS PAGE INTENTIONALLY LEFT BLANK

EXECUTIVE SUMMARY

A magnetic fuel cell uses high-pressure gas to cause a time-dependant change in magnetic field to generate a voltage based upon Faraday's Induction Law. In this thesis, the use of a compressed magnetic gas passing through a magnetic field is described for generation of electrical power.

The first stage of this thesis explores the fundamental physical nature of diamagnetic and paramagnetic gases. The ability of these gases to change their susceptibility as pressure changes was instrumental in producing voltage in the fuel cell. The basic equation explaining how susceptibility affects the magnetic field of a magnetic circuit is show in Equation (1.1),

$$B = \mu_o (1 + \chi) H . \tag{1.1}$$

The magnetic flux density, B, equals a constant (μ_o which is the permeability of free space) times the quantity one plus the susceptibility, χ, time the magnetic field strength, H. This equation explains how a change in susceptibility can affect the magnetic flux density of the magnetic circuit. The final component of the magnetic fuel cell concept is gas dynamics. Using Bernoulli's principle, the velocity of a high-pressure gas can be determined. Velocity of the high pressure gas and Equation (1.1) can be combined together and substituted into Faraday's Induction law to achieve a linear relationship between the voltage output of the fuel cell and the gas pressure.

Once the basic derivation was completed, it is clear that there are several methods that can be used to overcome the weak nature of diamagnetic and paramagnetic gases and achieve useful work. The second chapter of the thesis developed the theory used to model the operation and physical characteristics of the magnetic fuel cell. The predicted voltage output was 3.6 millivolts with a period of 3.7 milliseconds. A schematic of the test setup is shown in Figure 1. The largest challenge during this testing phase was reducing the noise floor and accounting for mechanical vibration produced by the discharge of the high-pressure gas.
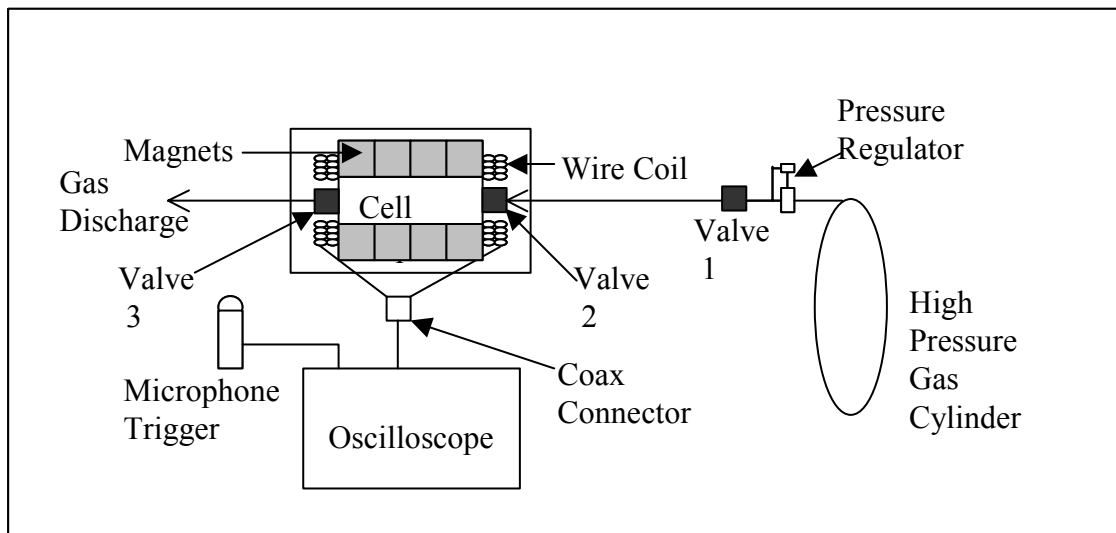
Figure 1   Schematic of Test Setup.

The schematic (Figure 1) shows the gas flow path for the high-pressure air. The gas
flows past the pressure regulator through valves one and two into the magnetic fuel cell.
The gas inside the fuel cell modulates magnetic flux inducing a voltage in the wire coil.
The oscilloscope records the voltage signal. The microphone triggers the oscilloscope to
start recording the signal. The isolated voltage signal of 6.3 millivolts produced by
discharging 1800 psi air out of the magnetic fuel cell as shown in Figure 2. The
sinusoidal pulse had a period of 0.3 milliseconds.
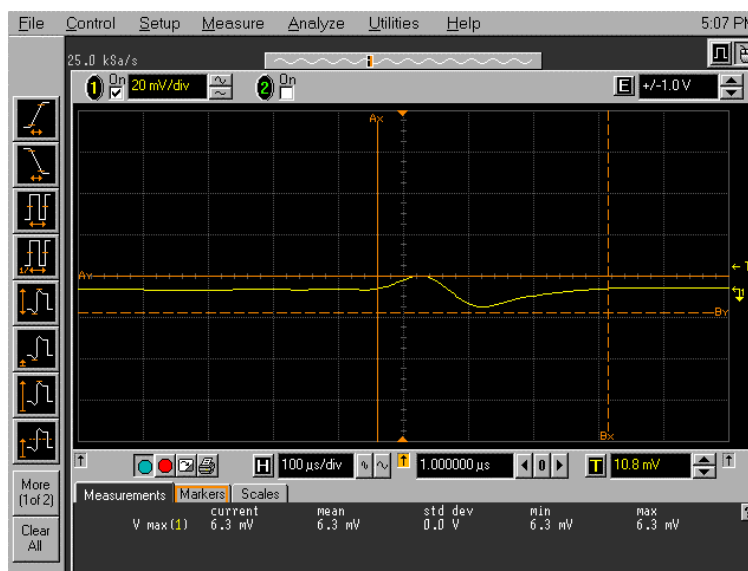
Figure 2   HP Oscilloscope Screen Capture of Magnetic Fuel Cell Output.

The vertical scale was 20 millivolts per division and the horizontal scale was 100 microseconds per division. The difference between theory and measured values was 3.6 millivolts, an error factor of 0.57. The predicted and measured voltage showed good agreement. The period of the actual signal was off by a factor of a hundred but agreed more closely with the manufactures calculations of 0.5 milliseconds.

Chapter V summarized the first three chapters and discussed a recommendation for the next experiment. Chapter V concluded with ramifications of the magnetic fuel cell. The magnetic fuel cell could be optimized to throttle and stop the high-pressure gas flow without physical contact. The equations for the magnetic fuel cell also could be applied to understanding weather; explaining weather effects such as lightening, storms, how wind is generated and how the ionosphere becomes electrically charged.

THIS PAGE INTENTIONALLY LEFT BLANK

I.   INTRODUCTION

Modern portable energy generation methods typically rely on chemical energy to produce electrical energy. Fuels, such as hydrogen, oxygen, diesel, and gasoline, are used to generate power for vehicles and other types of portable equipment. These methods bring several disadvantages; they are highly combustionable, explosive, toxic, and costly to produce. All generate environmentally unsafe waste products (e.g., CO, CO_2, NO_2 etc.).

Portable energy generation systems based upon chemical energy are very inefficient. After the chemical-based fuels release their energy, the energy must go through several conversions before being turned into electrical energy. For example, a turbine generator, found on many naval ships, has very low efficiency. The turbine generator process converts gasoline into mechanical energy by ignition (with some energy lost due to heat). The resulting mechanical energy is then channeled through turbine wheels where some of the energy is lost to friction and windage losses. The turbine axle rotates an electrical generator that has friction losses, hysteresis losses, and counter-induction losses. All these losses occur before useful electrical energy is developed. The total efficiency of the system can be found by multiplying individual loss efficiency terms together. The resulting total efficiency term for the turbine generator is very low.

The optimal heat engine, of which most chemical energy systems are a subcategory, also has a limit. This limit is based upon a concept called Carnot efficiency [1]. The Carnot efficiency is found by dividing the temperature difference between a heat source and a heat sink by the temperature of the heat source. Using a practical heat engine's temperature parameters, a heat engine could achieve a Carnot efficiency of approximately 45% [1].

The efficiency limitations of the heat engine are one of the main reasons electric fuel cells have been mandated by President Bush's administration as the technology of the future [2]. A fuel cell has a one-step conversion process that is not based upon a heat cycle and therefore does not have the Carnot efficiency limitation. Unfortunately, most electric fuel cells use hydrogen, which is explosive. This has affected the growth of this

technology in the commercial sector. The main research effort in industry has been the search for a safe, non-explosive, low-cost hydrogen storage tank to circumvent this issue. (Note: Appendix A discusses hydrogen-based electric fuel cells in detail.)

Instead of using chemical energy in a fuel cell, it is possible to use a magnetic gas. Direct conversion from mechanical energy into electrical energy is achieved. This fuel cell is called a magnetic fuel cell. Like the electric fuel cell, it is not a heat engine. Therefore, the theoretical efficiency could be much higher.

Magnetic devices and applications have experienced a tremendous growth commercially in the last forty years mainly due to the ability of industry to manufacture stronger and more powerful permanent magnets. In the early nineteenth century, permanent magnets were hard to obtain. Most scientists used direct-current transformers to achieve strong magnetic fields. Permanent magnets were only several hundred Gauss strong and weakly coercive. (Coercivity is defined as a property of magnetism, which relates to how resistant the magnet is to demagnetization by an external magnetic field.) Once the discovery of the Neodymium-Iron-Boron (abbreviated: Nd-Fe-B) and Samarium Cobalt (abbreviated: Sm-Co) rare earth magnets were made, magnetic flux densities rose within a few years to 10 to 20,000 Gauss (1 to 2 Tesla). The discovery of these rare earth magnets also allowed the size of the magnets to decrease without a decrease in strength and coercivity.

To achieve voltage induction without moving parts requires the development of a magnetic gas as the working medium. Magnetohydrodynamics (MHD) offers one solution. MHD uses ionized gasses and liquids as the working medium but this requires a method to ionize the gasses/liquids [3]. What about using a magnetic gas? The traditional method of manufacturing a permanent magnetic material involves the establishment of magnetic domains within the material. These magnetic domains in a gas would change a gas into either a liquid or solid. Magnetic liquids have been made using finely powered magnetic materials placed in an oil slurry. These liquids are employed effectively today as new generation shock absorbers on cars and as hydraulic lift replacements for carrier launch pads. The problem with a magnetic liquid is the difficulty in obtaining it and it is usually limited in quantity.

The only types of gas that exhibit magnetic properties are diamagnetic (e.g., nitrogen) and paramagnetic gases (e.g., oxygen). Diamagnetic gases are gases that are repelled from magnetic fields. The electrons in a diamagnetic material rearrange their orbits slightly, creating small persistent currents that oppose the external magnetic field. Paramagnetic gases are gases that are attracted towards magnetic fields. Both magnetic gases are weakly magnetic as categorized by their magnetic susceptibility (measure of a substance's ability to conduct a magnetic field). Paramagnetic gases are much stronger than diamagnetic gases.

A schematic of several energy transformation concepts is shown in Figure 1. This schematic shows that useful work from a heat engine begins as chemical energy and is converted using chemical combustion. The combustion energy then applies mechanical force to move a prime mover. The prime mover's energy is then electromagnetically converted to useful work.

♦ **Heat Engines – Carnot Efficiency**

| Chemical Combustion | → | Prime Mover | → | Electro-Magnetic Conversion | → | Work |

♦ **Hydrogen Fuel Cell**

| Hydrogen Storage | → | Hydrogen Diffusion | → | DC Current | → | Work |

♦ **Magnetic Fuel Cell**

| High Pressure Gas | → | Varying H Field | → | AC Current | → | Work |

♦ **Batteries**

| Chemical Storage | → | Electolytic Charge Transfer | → | DC Current | → | Work |
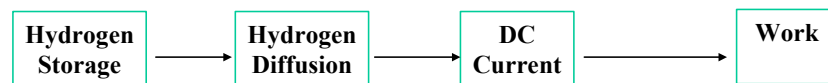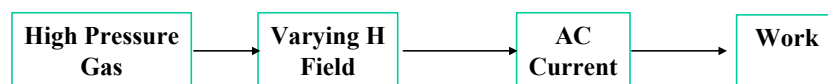
Figure 1   Energy Transformation Concepts.

The hydrogen fuel cell produces useful work by converting stored hydrogen catalytically into electrons and protons. The electrons flow through a circuit around the fuel cell and the protons diffuse through a proton exchange membrane. On the other side of the proton exchange membrane, the protons combine with air to produce water and heat. The electrons in the circuit produce a DC current, which provides work.

A magnetic fuel cell uses the varying susceptibility of high-pressure gases as its energy source. When exposed to a magnetic field, these gasses modulate the magnetic flux density and induce an AC voltage in a winding. The AC voltage is used to produce work.

Finally, a battery is used to store chemical energy. The chemical energy is released upon closure of the electrical circuit via electrolytic charge transfer. A DC current is produced which is used for work.

With an understanding of the energy transformation process, Chapter II addresses how the varying susceptibility of high-pressure gases produces work. Chapter II begins with the theoretical explanation of magnetism and gas dynamics and finishes with a presentation of the magnetic fuel cell concept. Chapter III starts with a full theoretical development, including the magnetic circuit. A discussion is included in optimizing the number of windings of the magnetic fuel cell. Chapter III ends by discussing implementation considerations of the experiment and experimental predictions. Chapter IV addresses the experimental setup and includes an analysis of the data. Chapter IV concludes with a discussion of the lessons learned from the experiment. Chapter V provides a conclusion with several recommendations regarding future work and a few ramifications of the magnetic fuel cell concept.

II. BACKGROUND THEORY

This Chapter develops the underlying physical principles of how a magnetic fuel cell works. The first section discusses magnetism. Specifically, it describes magnetic materials and their classification, the concept of coercivity and susceptibility, the hysteresis loop, and magnetic circuits. The next section discusses gas flow dynamics, Bernoulli's principle, the continuity equation and how to estimate gas velocities. Section C describes Faraday's Induction law, showing how to achieve a voltage using a change in the magnetic field. The final section introduces the basic theoretical idea of the magnetic fuel cell. It will show how magnetism, gas dynamics and Faraday Induction concepts are combined together to achieve the overall concept.

A. MAGNETISM

One fundamental force of nature is magnetic force, a property of magnetism. Magnetism allows the application of force at a distance and the ability to connect two metallic objects without using physical fasteners. To understand what makes a material magnetic requires the development of two magnetic concepts, atomic magnetism and molecular magnetism.

Atomic magnetism focuses on the structure of the atom. An atom is made up of neutrons and protons in the nucleus and electrons orbiting the nucleus. The electrons have a property called spin. This property has been identified as the essential ingredient to producing magnetic fields. Spin can be broken down into two states, spin up and spin down. An elementary rule of electron spin is that electrons like to pair up with one spin-down electron and one spin-up electron. When an electron does not pair up, the element will be considered magnetic. Most elements are not magnetic. Typically unpaired electrons are in the atom's outer orbit. These electrons pair up with electrons from other atoms forming non-magnetic molecules. The exception to this is the magnetic elements, two of which are iron and nickel. Iron, for example, is magnetic because there are several unpaired electrons in its 3D atomic shell. The outer shell of Iron is 4S. The outer shell acts as a shield for the D shell electrons preventing pairing of electrons from other atoms. However, not all iron materials are magnetic due to molecular magnetism.

When atoms combine into molecules, or form into crystals, only certain magnetic orientations are allowed. Two adjacent atoms with unpaired D shell electrons will have magnetic fields pointing in parallel but opposing directions. This effectively cancels out the net magnetic field. Thermal noise constantly overpowers the weak magnetic fields of individual atoms. The material then develops regions or domains within it that are magnetically polarized in different directions with no overall magnetic field. Only certain materials exposed to an external magnetic field will retain a residual magnetic field after the external magnetic field is removed.

1.   **Magnetic Materials**
     (a)   Classification

The following categories show how a magnetic material is classified.

- Ferromagnetic materials are materials in which magnetic domains align to form a residual magnetic field. This magnetic field will exist without an external field applied. One example of this is iron. Iron has four unpaired electrons in its atomic D shell, which are protected by an outer shell. These electrons have the same spin state (up or down), producing a strong magnetic field.

- Anti-ferromagnetic materials are materials in which internal molecular magnetic fields align in parallel but opposite directions. The result is a zero net magnetic field. It is very difficult to change this magnetic field using an external magnetic source. This molecular phenomenon can be seen, for example, in copper atoms in a metallic lattice.

- Diamagnetic materials are materials that have no internal magnetic field. When an external magnetic field is applied, internal magnetic fields are generated to repel the external field. The atoms within these materials have no unpaired electron spins. Bismuth, having the largest number of paired electrons in the periodic table, is the strongest diamagnetic material. Striated carbon has been reported as stronger but only in one crystal plane [4].

- Paramagnetic materials are materials where a majority of atoms have magnetic fields aligned in different directions due to thermal noise. This

produces a zero net magnetic field. When an external field is applied, these internal magnetic fields slightly align. Oxygen is one element that is paramagnetic.

- Ferri-magnetic materials are materials where an external magnetic field will cause massive alignment of internal magnetic fields until the external magnetic field is removed. Elements such as manganese, aluminum and cobalt are ferri-magnetic.

(b)   Soft or Hard Magnetic Materials

Magnetic materials are classified as soft or hard depending on their coercivity (H_c), and permeability (μ). Coercivity was defined in Chapter I. A material with a high coercivity will require a large external magnetic field to reverse its magnetic polarization. A material with low coercivity will require a small external magnetic field to reverse its polarization. Permeability is a constant of proportionality between magnetic flux density and magnetic field strength. It shows how effectively a material channels a magnetic field. Hard materials have a low permeability and a high coercivity (H_c>10000 A/m) [5]. Soft materials have a high permeability and low coercivity (H_c<1000 A/m) [5]. For the magnetic fuel cell, the materials of interest are soft magnetic materials. The magnetic fuel cell is designed to operate in the kHz range with a constantly changing magnetic field. Therefore, materials with high permeability, but very low coercivity, are desirable.

2.   Susceptibility

A measure of a material's ability to repel an external magnetic field is called susceptibility (χ). Susceptibility is unit-less and seen in Equations (1.1) and (1.2); as either relating to relative permeability (μ_r) or a constant of proportionality between magnetic flux density (B) and magnetic field strength (H),

$$\mu_r = 1 + \chi ,$$ (1.1)

$$B = \mu_o \mu_r H ,\qquad(1.2)$$

where μ_o is the relative permeability of free space $\left(\mu_o \left[\dfrac{\text{kg-m}}{\text{A}^2\text{-s}^2} \right] = 4\pi \times 10^{-7} \right)$.

Experimental susceptibility (κ) has units of cm^3/mol. The equation for experimental susceptibility is (MKS),

$$\kappa = \chi \frac{M}{4\pi\rho} ,\qquad(1.3)$$

where:

- M is the molar mass (g/mol) and

- ρ is the material density.

The basic equation that relates magnetic flux density (B) to magnetic field strength (H) and magnetization (M) is:

$$B = \mu(H + M) .\qquad(1.4)$$

Susceptibility is related to the basic magnetic equation by observing,

$$\mu = \mu_o \mu_r ,\qquad(1.5)$$

where μ is magnetic permeability.

The form used herein will be:

$$B = \mu_o(1 + \chi)H .\qquad(1.6)$$

(a)   Diamagnetism

In diamagnetic materials, susceptibility values are negative and very small ($\chi \approx -10^{-9}$ [1]). The strongest diamagnetic material is striated carbon, $\chi \approx -0.00142$ [4]. There are several diamagnetic gases, a few examples include: fluorine, steam, and the noble gases. Nitrogen has a susceptibility of $\chi = -5.4 \times 10^{-9}$ [6] at room temperature and pressure. Plasma is considered weakly diamagnetic with a susceptibility close to that of nitrogen. Since diamagnetism occurs at the atomic level, quantum mechanics is used to explain the theory of diamagnetism. Materials become more diamagnetic as size shrinks

towards the atomic state. Susceptibility can be calculated using the following equation [7],

$$\chi = \frac{-\mu_o N_v Z q^2 < r^2 >}{6 m_e},$$ (1.7)

where:

- N_v is atoms per unit volume,

- q is the electron charge $\left(q = 1.6 \times 10^{-19} \text{coulombs} \right)$,

- $< r^2 >$ is the expectation value of the orbital area $\left(\text{m}^2 \right)$,

- Z is atomic number of the element and

- m_e is electron mass $\left(m_e = 9.1 \times 10^{-31} \text{kg} \right)$.

Susceptibility is therefore proportional to atoms per unit volume. The susceptibility equation predicts that, by keeping volume/temperature constant, a steadily increasing pressure will cause a steadily increasing susceptibility. Nitrogen is a gas that makes up approximately 80 percent of the Earth's atmosphere. Figure 2 shows pressure versus susceptibility for diamagnetic materials: nitrogen (N_2), bromine (Br_2), bismuth (Bi); and the paramagnetic gas, oxygen (O_2). As pressure and susceptibility increase, bromine's susceptibility becomes larger than bismuth. Nitrogen, on the other hand, must be pressurized to several million psi before becoming stronger than bismuth. In contrast to these diamagnetic gases, oxygen is paramagnetic and an order of ten to a thousand times as strong as the diamagnetic materials. Oxygen in the form of pressurized air will be used in the magnetic fuel cell experiment for this reason.
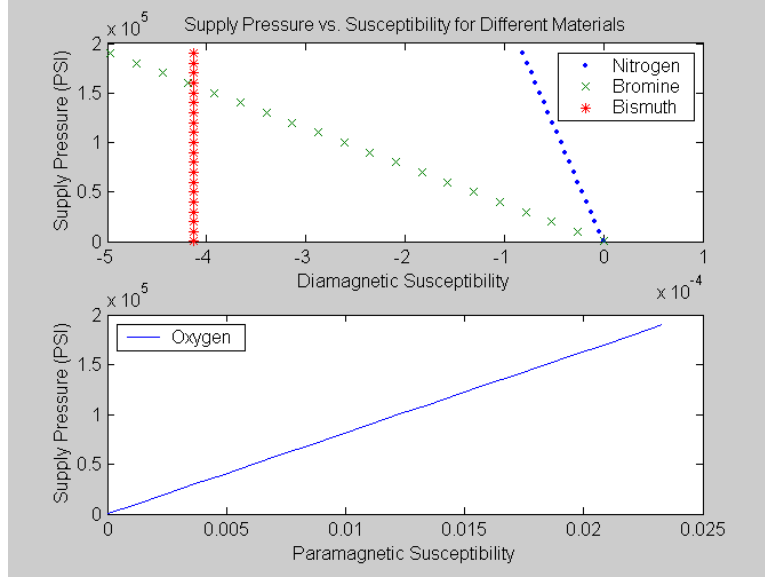
Figure 2   Gas Pressure versus Susceptibility for Common Gases (Bismuth Included).

(b)   *Paramagnetism*

Air is the predominant paramagnetic gas. Comprised of 19 percent oxygen and 80 percent nitrogen, the highly paramagnetic effect $\left(\chi = 1.87 \times 10^{-6} \right)$ of oxygen overcomes the small diamagnetic effect ($\chi = -5.4 \times 10^{-9}$) of nitrogen. Paramagnetic gases are temperature dependant. Hence, heating air to approximately $300\ ^{o}F$ will cause oxygen to become diamagnetic. This change in susceptibility due to temperature or pressure will be key in achieving the optimal fuel cell design. The quantum mechanical equations for paramagnetism are given in Equation (1.8) [7, 8], for two situations. The first situation calculates susceptibility based upon changing pressure with a fixed temperature. The second situation calculates susceptibility based upon increasing temperature [8]. Note that the second situation shows how a paramagnetic material becomes diamagnetic upon increased temperature.

$$\chi_p = \begin{cases} 7.1 \times 10^{-32} N_v & T = 293\ K \\ \dfrac{\mu_m^2}{K_B T} \left[\left(\dfrac{K_B T}{\mu_m H} \right)^2 - \csc h^2 \left(\dfrac{\mu_m H}{K_B T} \right) \right] & T > 293 K \end{cases} \qquad (1.8)$$

where:

- μ_m is the magnetic moment of the atom,

10

- K_B is Boltzmann constant and

- T is temperature (Kelvin).

3. Polarity

Magnetic fields exhibit a permanent dipole state. There is always a north and south pole. Convention states that the north pole is the source and the south pole is the sink. Homogenous magnetic fields are a key ingredient in the magnetic fuel cell. Since diamagnetic gases will collect in regions of lowest magnetic field strength, a homogenous field must be present to ensure the gas stays within the maximum field region.

4. Hysteresis

For anyone wanting to work with magnetism, understanding magnetic hysteresis is essential.

> When a ferromagnetic material is magnetized in one direction, (Figure 3) it will not relax back to zero magnetization when the imposed magnetizing field is removed. It must be driven back to zero by a field in the opposite direction. If an alternating magnetic field is applied to the material, its magnetization will trace out a loop called a hysteresis loop. The lack of retraceability of the magnetization curve is the property called hysteresis and it is related to the existence of magnetic domains in the material. Once the magnetic domains are re-oriented, it takes energy to turn them back again. This property of ferromagnetic materials is useful as a magnetic "memory." Some compositions of ferromagnetic materials will retain an imposed magnetization indefinitely and are useful as "permanent magnets." The magnetic memory aspects of iron and chromium oxides make them useful in audio tape recording and for the magnetic storage of data on computer disks. [9]
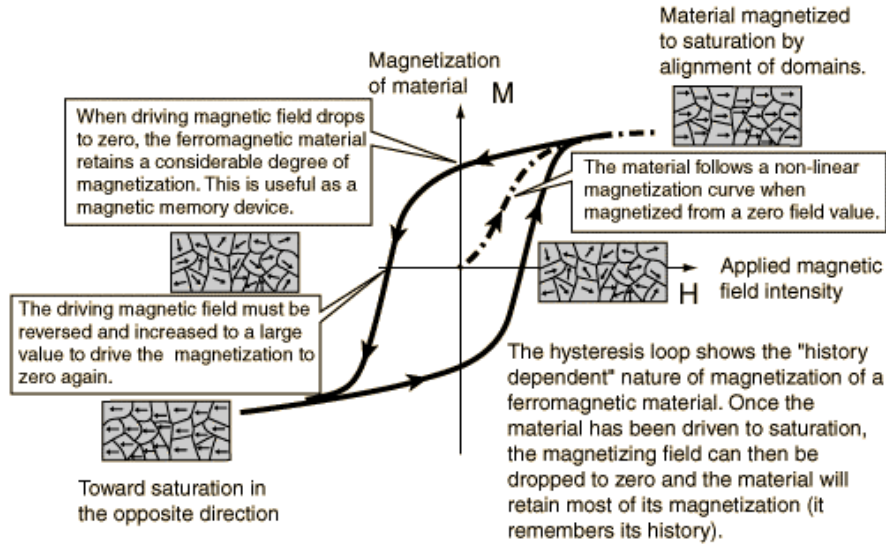
Figure 3   Hysteresis Curve (from [9]).

5.   Magnetic Circuits

Magnetic circuit configurations are used in transformers and electrical machines. *Magnetic circuit analysis* techniques are analogous to those of electrical circuits. The magneto-motive force (mmf) of an n-turn current-carrying coil is given by [5]:

$$\Im = \int \vec{H} \cdot d\vec{L} = nI \rightarrow \Im = H_c L_c + H_g L_g = nI ,\tag{1.9}$$

where:

- $\Im$ is the magneto-motive force,

- $d\vec{L}$ is change in unit length,

- n is number of windings,

- I is the induced current,

- H_c is core magnetic field strength,

- L_c is core length,

- H_g is gap magnetic field strength and

- L_g is gap length.

A current-carrying coil is the magnetic circuit equivalent to a voltage source in an electrical circuit. Therefore, magneto-motive force can be considered to be analogous to a

12

source voltage. The reluctance $(\Re)$ of a path for magnetic flux, such as the bar or iron is given by,

$$\Re = \frac{1}{\mu A},$$ (1.10)

where A is the cross-sectional area of the magnetic material. Reluctance is analogous to resistance in an electrical circuit. When the bar is not straight, the length of the path is taken to be the length of the centerline. Therefore, L_c is considered as the *mean length of the core path*. Magnetic flux (ϕ) in a magnetic circuit is equivalent of current in an electrical circuit. Magnetic flux, reluctance ($\Re$), and magneto-motive force are related by

$$\Im = \Re \phi.$$ (1.11)

This is analogous to Ohm's Law,

$$V = IR,$$ (1.12)

where:

- V is voltage and

- R is resistance.

The advantage of the magnetic circuit approach is that it can be applied to unsymmetrical magnetic cores with multiple coils. Coils are sources of magnetomotive forces that can be manipulated, in the same way voltage sources are in electrical circuits. Reluctances add in series or in parallel, just the same as resistance. Fluxes are analogous to currents. The magnetic circuit approach is not an exact method for determining magnetic fields. However, this approach is sufficiently precise for many engineering applications [5].

B.   GAS DYNAMICS

Gases at high-pressure travel to areas of low pressure, this is according to Bernoulli's principle [1], Equation (1.13). These equations can be further broken down as shown in Equations (1.14)-(1.16),

13

$$\Delta E_{KE} + \Delta E_{PE} + \Delta E_{gas} = 0, \tag{1.13}$$

$$\Delta E_{KE} = \frac{1}{2}m(v_f^2 - v_i^2), \tag{1.14}$$

$$\Delta E_{PE} = mg(h_f - h_i) \text{ and} \tag{1.15}$$

$$\Delta E_{gas} = V_g(P_f - P_i). \tag{1.16}$$

where:

- ΔE_{KE} is change in kinetic energy of the gas,

- ΔE_{PE} is the change in gravitational potential energy of the gas,

- ΔE_{gas} is the change in pressure energy of the gas,

- v_f is the final velocity of the gas,

- v_i is the initial velocity of the gas,

- g is gravity (9.8 m/s^2),

- h_f is final height,

- m is the mass of the gas,

- h_i is initial height,

- V_g is volume of the gas,

- P_f final steady state pressure of the gas, and

- P_i is the initial pressure of the gas.

Re-arranging Bernoulli's principle, the final velocity of the gas can be solved for as seen in Equation (1.17). The velocity of the gas is proportional to the square root of the change in pressure divided by the density change,

$$v = \sqrt{\frac{2\Delta P}{\rho}}, \tag{1.17}$$

where v is gas velocity and ΔP is change in pressure of the gas.

14

For an ideal gas, the equation of state [1] is Equation (1.18). Pressure can be determined using Equation (1.19). The mass of the gas can be solved using Equation (1.20). Finally, using Equations (1.21) and (1.22), the gas density is solved for in Equation (1.22),

$$PV_g = n_m RT , \qquad (1.18)$$

$$P = \frac{n_m RT}{V} , \qquad (1.19)$$

$$m = n_m M , \qquad (1.20)$$

$$\rho = \frac{m}{V} , \qquad (1.21)$$

$$\rho = \frac{PM}{RT} , \qquad (1.22)$$

where: n_m is the number of moles and R is the universal gas constant $\left(R = 8.314 \text{ J}/\left(\text{mol-K}\right) \right)$. Since the gas is pulsated into a chamber at close to one-millisecond time intervals there is not enough time for heat transfer to occur. Therefore, this process can be analyzed adiabatically by the following Equation [1],

$$PV_g^\gamma = \text{constant}, \qquad (1.23)$$

where γ is the ratio of molar specific heats ($\gamma = 1.4$ for diatomic molecules).

C.   FARADAY'S LAW

Faraday's law states that the line integral of the electric field around a stationary loop equals the negative surface integral of the time rate of change of the magnetic flux density B integrated over the loop area [10]. For a fuel cell, the voltage induced reduces to

$$V = -n\frac{\Delta\phi}{\Delta t} = -n\frac{\Delta BA}{\Delta t}, \qquad (1.24)$$

where:

- $\Delta\phi$ is the change in magnetic flux,

15

- Δt is the change in time and

- ΔB is the change in magnetic flux density.

D.   BASIC CONCEPT

From the previous theory, the basic equation development of the fuel cell. Figure 4 shows the conceptual operation of a fuel cell is presented. (Note, for explanatory purposes flux lines are shown doubling in the soft magnetic core vice; in reality, the doubling occurs in the magnetic fringe around the magnets.) At time zero, the diamagnetic gas volume is outside the gap. At time one, the diamagnetic gas enters the gap and suppresses the local magnetic field. Since magnetic flux is conserved, the magnetic flux in the soft magnetic core doubles. This change in flux induces a voltage in the coil. At time two, the diamagnetic gas volume has reduced in the gap. The flux is no longer sup-pressed, thus causing the flux in the core to decrease by one half. This change in flux induces a negative voltage in the coil. The process then repeats at time one.
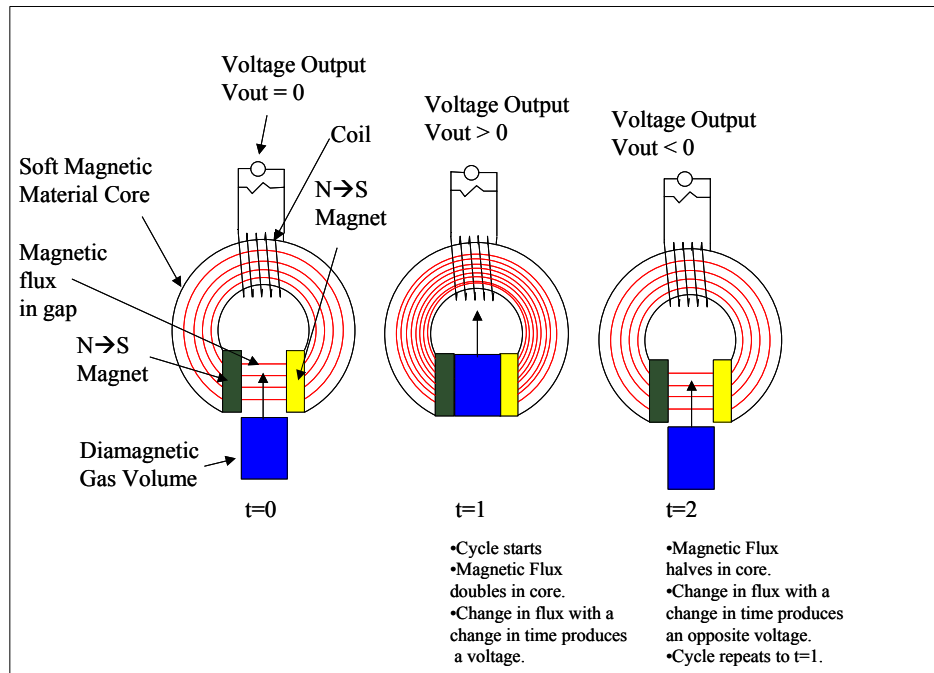
Figure 4   Conceptual Operation of the Magnetic Fuel Cell.

Voltage is induced by a change in flux inside a coil of n turns, Equation (1.25). A change in flux is proportional to a change in magnetic flux density times the area,

16

$$V = -n\frac{\Delta\phi}{\Delta t} = -n\frac{\Delta BA}{\Delta t}.$$ (1.25)

The magnetic flux density is given by

$$B = \mu_o(1 + \chi)H.$$ (1.26)

Therefore, a change in magnetic flux density will be the difference between the initial susceptibilities and magnetic field strengths and final susceptibilities and magnetic field strengths,

$$\Delta B = \mu_o(1 + \chi_f)H_f - \mu_o(1 + \chi_i)H_i \approx \mu_o H \Delta\chi,$$ (1.27)

where:

- χ_f is the final susceptibility,

- χ_i is the initial susceptibility,

- $\Delta\chi$ is the change in susceptibility,

- H_f is the final magnetic field strength, and

- H_i is the initial magnetic field strength.

For this basic derivation the final and initial magnetic field strengths are assumed to be equal. This will not be assumed for the advanced derivation shown in Chapter III.

Substituting Equation (1.27) into Equation (1.25), the voltage is now shown to be proportional to the change in susceptibility,

$$V = -n\frac{\mu_o H \Delta\chi A}{\Delta t}.$$ (1.28)

The unit-less susceptibility, χ, is shown to be proportional to the experimental susceptibility, κ, by

$$\kappa = \chi\frac{M}{4\pi\rho} \rightarrow \chi = \frac{4\pi\rho\kappa}{M}.$$ (1.29)

The difference in susceptibility using Equation (1.29) becomes Equation (1.30) and is now proportional to the change in density of the gas,

$$\Delta\chi = \frac{4\pi\rho_f\kappa}{M} - \frac{4\pi\rho_i\kappa}{M} = \frac{4\pi}{M}\left[\rho_f - \rho_i\right]. \tag{1.30}$$

Substituting Equation (1.30) into (1.28) leads to

$$V = -n\frac{\mu_o H \frac{4\pi}{M}\left[\rho_f - \rho_i\right]A}{\Delta t}, \tag{1.31}$$

where voltage is proportional to the change in density of the gas. The density of the gas can be related to pressure

$$\rho = \frac{PM}{RT}. \tag{1.32}$$

(The assumption that the gas is ideal is for the simplified case and is treated more rigorously in Chapter III.) Substituting (1.32) into (1.31) shows voltage is proportional to change in pressure of the gas,

$$V = -4\pi n\frac{\mu_o H}{RT}A\frac{\Delta P}{\Delta t}. \tag{1.33}$$

The time it takes the gas to change pressure is equal to the height of the fuel cell divided by the velocity of the gas (v),

$$\Delta t = \frac{h}{v}, \tag{1.34}$$

where h is the height of the gap.

From Bernoulli's principle the velocity of gas is proportional to the square root of two times the change in pressure of the gas divided by the density of the gas. Using Equation (1.22), density can be changed into equivalent pressure, P_i to give

$$v = \sqrt{\frac{2\Delta P}{\rho}} = \sqrt{\frac{2RT}{M}\frac{\Delta P}{P_i}}. \tag{1.35}$$

(Note: Equation (1.35) has been simplified for the basic derivation; a more complete analysis is in Chapter III.) Substituting Equations (1.34) and (1.35) into (1.33) produces

$$V = -4\pi n\frac{\mu_o H}{\sqrt{RT}}A\frac{\Delta P^{\frac{3}{2}}}{h}\sqrt{\frac{2}{MP_i}}. \tag{1.36}$$

18

Assuming the initial pressure is much greater than final pressure and substituting in for area (A) of the fuel cell we find

$$V = -4\pi n \mu_o H w \Delta P \sqrt{\frac{2}{MRT}} \; .$$

(1.37)

As seen from Equation (1.37), voltage is produced from a change in pressure of a gas. Voltage is primarily optimized by: 1) maximizing the pressure change, ΔP; 2) maximizing the number of turns of the coil, n; 3) maximizing width of the fuel cell, w; and 4) maximizing the magnetic field strength in the gap, H.

This Chapter has introduced the basic concepts required to understand how a magnetic fuel cell functions. Extensive discussion of magnetic properties was reviewed, along with gas dynamics. Using these concepts, the basic equation for the fuel cell was derived showing its dependency on gas pressure, magnetic field strength, and fuel cell geometry. Chapter III will present, a more thorough analysis of the magnetic fuel cell, a discussion and derivation of coil optimization, and what the implementation issues were for the experiment.

THIS PAGE INTENTIONALLY LEFT BLANK

III.   EXPERIMENTAL SETUP

A.   THEORETICAL DEVELOPMENT

This Chapter will discuss the detailed derivation of the magnetic fuel cell. Two key parameters that will be solved are the static magnetic field inside the pressure chamber and the change in magnetic field due to the pressure change. These parameters affect the magnitude of the voltage in the fuel cell equation. The next Section discusses the optimization of power. The final Section of Chapter III will apply the detailed derivation to the experiment model.

The geometric configuration of the magnetic fuel cell is shown in Figure 5. A stable DC magnetic field is generated using Nd-Fe-B permanent magnets. These magnets are placed on the ends of highly permeable, high frequency, soft magnetic material (called a c-core). A pressure chamber fits inside the gap between the magnets. High-pressure gas flows into and out of the cylinder as controlled by valves two and three. The change in magnetization of the gas in the gap is caused by a change in pressure of the gas. The change in magnetization causes a change in magnetic flux. This change in magnetic flux induces a voltage in a coil wound around the c-core soft magnetic material. The induced voltage is applied to the load resistance.
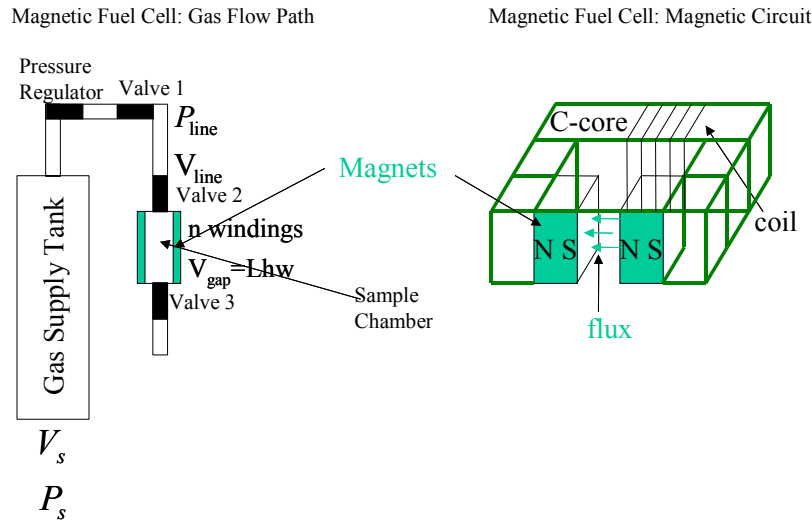
Figure 5   Magnetic Fuel Cell Gas and Magnetic Conceptual Flow Paths.

The first part of the derivation is a three-step development to determine the time the gas takes to enter the chamber and exit the chamber. (Note: that the viscosity effects and heating effects of the gas are ignored in this derivation due to the small length of piping the gas travels through and the short time the gas takes to discharge to the atmosphere.) The first step is to determine the time for the gas to enter the gas chamber using Bernoulli's principle,

$$\frac{P_s}{\rho_s} + \frac{v_s^2}{2} = \frac{P_{gap1}}{\rho_{gap1}} + \frac{v_{valve2}^2}{2},$$

(2.1)

where:

- v_{valve2} is the velocity of the gas entering valve two,

- v_s is the velocity of the gas in the supply tank,

- P_s is the pressure of the gas in the supply tank,

- ρ_s is the density of the gas in the supply line,

- P_{gap} is the pressure of the gas in the gap, and

- ρ_{gap} is the density of the gas in the gap.

Using Bernoulli's principle [1], the velocity of the gas traveling through valve two is determined by,

$$v_{valve2} = \sqrt{2\left(\frac{P_s}{\rho_s} - \frac{P_{gap}}{\rho_{gap}}\right)}.$$

(2.2)

Next, the final velocity of the gas entering the pressure chamber is determined using the continuity equation [1],

$$\rho_s A_{valve2} v_{valve2} = \rho_{gap} A_{gap} v_{gap-in},$$

(2.3)

where:

- A_{valve2}, the cross-sectional area of valve two,

- A_{gap}, the cross-sectional area of the gas chamber and

22

- v_{gap-in} , the velocity of the gas entering the gap.

The supply volume, V_s , is much larger than the gap volume, V_{gap}. The density of the line equals the density of the gap. Rearranging Equation (2.4) produces

$$v_{gap-in} = \frac{A_{valve2}}{A_{gap}} v_{valve2} . \tag{2.5}$$

The time for the gas to enter the gas chamber is,

$$\Delta t_{in} = \frac{h_{gap}}{v_{gap-in}} , \tag{2.6}$$

where h_{gap} is the height of the gas chamber. Substituting, Equation (2.5) and (2.2) into (2.6) produces

$$\Delta t_{in} = \frac{h_{gap}}{\frac{A_{valve2}}{A_{gap}} \sqrt{2 \left(\frac{P_s}{\rho_s} - \frac{P_{gap}}{\rho_{gap}} \right)}} . \tag{2.7}$$

The second step is to determine the time for the gas to exit the gas chamber. Applying Bernoulli's principle and solving for the velocity of the gas entering valve three,

$$\frac{P_{gap}}{\rho_{gap}} + \frac{v_{gap-out}^2}{2} = \frac{P_{atm}}{\rho_{atm}} + \frac{v_{valve3}^2}{2} , \tag{2.8}$$

$$v_{valve3} = \sqrt{2 \left(\frac{P_{gap}}{\rho_{gap}} - \frac{P_{atm}}{\rho_{atm}} \right)} , \tag{2.9}$$

where:

- v_{valve3} is the velocity of the gas entering valve three,

- $v_{gap-out}$ is the velocity of the gas leaving the gap,

- P_{atm} is atmospheric pressure, and

- ρ_{atm} is atmospheric density.

23

Next, the final velocity of the gas exiting the pressure chamber is determined using the continuity equation,

$$\rho_{atm} A_{valve3} v_{atm} = \rho_{gap} A_{gap} v_{valve3}, \tag{2.10}$$

where A_{valve3} is the cross sectional area of valve two and v_{atm} is the velocity of the gas exiting valve two. Rearranging terms and solving for atmospheric velocity,

$$v_{atm} = \frac{\rho_{gap} A_{gap} v_{valve3}}{\rho_{atm} A_{valve3}}. \tag{2.11}$$

The time for the gas to exit the gas chamber, Δt_{out}, is,

$$\Delta t_{out} = \frac{h_{gap}}{v_{atm}}. \tag{2.12}$$

Substituting, Equation (2.9) and (2.11) into (2.12) gives

$$\Delta t_{out} = \frac{\rho_{atm} A_{valve3}}{\rho_{gap} A_{gap}} \frac{h_{gap}}{\sqrt{2\left(\dfrac{P_{gap}}{\rho_{gap}} - \dfrac{P_{atm}}{\rho_{atm}}\right)}}. \tag{2.13}$$

The third step is to determine the total time of operation of the magnetic fuel cell. This process will include the time taken to cycle open and shut valves two and three. The cycle time is the sum of the valve operation times and charge and discharge times,

$$t_{cycle} = \Delta t_{in} + t_{valve2} + \Delta t_{out} + t_{valve3}, \tag{2.14}$$

where:

- t_{cycle} is the cycle time of the magnetic fuel cell,

- t_{valve} is the time to open and shut valve two, and

- t_{valve3} is the time to open and shut valve three.

The cycle frequency, f_{cycle}, is

$$f_{cycle} = \frac{1}{t_{cycle}}. \tag{2.15}$$

The volume flow rate of the cycle, $\dot{V}_{cycle}$, is

$$\dot{V}_{cycle} = \frac{V_{gap}}{t_{cycle}}. \qquad (2.16)$$

The duration or total time it takes for the supplying high-pressure gas tank to become exhausted, t_d, is

$$t_d = \frac{V_s}{\dot{V}_{cycle}}. \qquad (2.17)$$

The timing of the fuel cell has been determined. The next series of steps analyzes the magnetic circuit (Figure 5) of the magnetic fuel cell. This analysis begins with the determination of the magnetic load line. From the static magnetic field equations, the circulation of magnetic field strength per unit length is equal to the integral of the current density per unit area,

$$\int H \, dL = \int_S J \, ds = nI, \qquad (2.18)$$

where J is the induced current density in the set of windings, and ds is the unit area perpendicular to the magnetic flux lines. The circulation of the magnetic flux density around a closed surface is zero,

$$\oint_S \vec{B} \cdot d\vec{s} = 0. \qquad (2.19)$$

(Assumption: the flux generated by the field source is confined to the magnetic circuit with minimal leakage.) Equation (2.20) becomes

$$H_m L_m + H_{gap} L_{gap} + H_{core} L_{core} = nI, \qquad (2.20)$$

where:

- H_m is the magnet magnetic field strength,

- L_m is the length of the magnets,

- H_{gap} is the gap magnetic field strength,

25

- L_{gap} is the length of the gas chamber or gap,

- H_{core} is the core magnetic field strength, and

- L_{core} is the length of the core.

The magnetic flux through a surface is zero as shown by Equation (2.19). The magnetic flux densities for each component are therefore equal (assuming fringing flux is small),

$$B = B_{gap} = B_{core} = B_m ,$$ (2.21)

where:

- B_{gap} is the gap magnetic flux density,

- B_{core} is the core magnetic flux density and

- B_m is the magnet magnetic flux density.

The basic equation for magnetic field strength becomes (Note: the derivation of Equation (2.25) is covered in Appendix B.),

$$H = \frac{B}{\mu_o \mu_r} ,$$ (2.22)

$$H_{gap} = \frac{B}{\mu_{gap} \mu_o} ,$$ (2.23)

$$H_{core} = \frac{B}{\mu_{core} \mu_o} ,$$ (2.24)

$$I = \frac{Bk}{\mu_o} ,$$ (2.25)

$$k = \frac{\pi w_c h_c}{2 \mu_{core} \sqrt{h_c^2 + w_c^2}} ,$$ (2.26)

where:

- μ_{gap} is the gas permeability within the gas chamber,

- μ_{core} is the core permeability,

- k is a simplification constant,

- h_c is the core height, and

- w_c is the core width.

Assuming the magnet has a linear second quadrant demagnetization curve, then the equation is of the form [5],

$$B_m = B_r + \mu_m H_m ,$$ (2.27)

and the magnetic permeability is defined by,

$$\mu_m = \frac{B_r}{H_c} ,$$ (2.28)

where:

- B_r is the residual magnetization,

- μ_m is the permeability of magnet and

- H_c is the magnet coercivity.

Setting magnetic flux densities equal to each other, Equations (2.27) and (2.28) allow the calculation of the magnetic load line. Substituting for magnetic field strength from Equations, (2.22)-(2.25), into Equation (2.20) produces Equation (2.29),

$$-H_m L_m = \frac{2B}{\mu_{gap}\mu_o} L_{gap} + \frac{B}{\mu_{core}\mu_o} L_p - n\frac{Bk}{\mu_o} .$$ (2.29)

Rearranging Equation (2.29) to solve for magnetic flux density produces,

$$B = -\frac{\mu_o H_m L_m}{\dfrac{L_{gap}}{\mu_{gap}} + \dfrac{L_{core}}{\mu_{core}} - nk} .$$ (2.30)

Setting Equation (2.27) equal to Equation (2.30) finds the magnetic field strength of the magnets,

$$B_r + \frac{B_r}{H_c} H_m = -\frac{\mu_o H_m L_m}{\dfrac{L_{gap}}{\mu_{gap}} + \dfrac{L_{core}}{\mu_{core}} - nk}$$

$$H_m = \frac{-B_r}{\dfrac{\mu_o L_m}{\dfrac{L_{gap}}{\mu_{gap}} + \dfrac{L_{core}}{\mu_{core}} - nk} + \dfrac{B_r}{H_c}}.$$

(2.31)

The flux through a surface, ϕ, is given by

$$\phi = \int_S \vec{B} \cdot d\vec{s}.$$

(2.32)

The area of the circuit is fixed. Equation (2.32) will reduce to

$$\phi = BA,$$

(2.33)

where A is the cross-sectional area of magnets.

Faraday's Induction equation describes the voltage induced into the windings by the change in flux in the gas chamber (repeated here for convenience),

$$V = -n \frac{\Delta \phi}{\Delta t}.$$

(2.34)

Substituting magnetic flux density from the load line equation into Faraday's Equation produces Equation (2.35) for the gas entering the chamber and Equation (2.36) for the gas discharging from the chamber,

$$B_{in} = -\frac{\mu_o H_m L_m}{\dfrac{L_{gap}}{\mu_{gap1}} + \dfrac{L_{core}}{\mu_{core}} - nk},$$

(2.35)

$$B_{out} = -\frac{\mu_o H_m L_m}{\dfrac{L_{gap}}{\mu_{gap2}} + \dfrac{L_{core}}{\mu_{core}} - nk},$$

(2.36)

where B_{in} is the magnetic flux density at high pressure and B_{out} is the magnetic flux density at atmospheric pressure.

The change in magnetic flux density becomes,

$$\Delta B = -\frac{\mu_o H_m L_m}{\dfrac{L_{gap}}{\mu_{gap2}} + \dfrac{L_{core}}{\mu_{core}} - nk} + \frac{\mu_o H_m L_m}{\dfrac{L_{gap}}{\mu_{gap1}} + \dfrac{L_{core}}{\mu_{core}} - nk}. \tag{2.37}$$

Substituting Equation (2.37) into (2.34) and using (2.33), the voltage can be determined,

$$V = \mu_o n H_m L_m A \left(\frac{\dfrac{1}{\Delta t_{in}}}{\dfrac{L_{gap}}{\mu_{gap1}} + \dfrac{L_{core}}{\mu_{core}} - nk} - \frac{\dfrac{1}{\Delta t_{out}}}{\dfrac{L_{gap}}{\mu_{gap2}} + \dfrac{L_{core}}{\mu_{core}} - nk} \right). \tag{2.38}$$

Using Equations (2.7) and (2.13) to substitute for time produces

$$V = \mu_o n H_m \frac{L_m}{h_{gap}} A \left(\frac{\dfrac{A_{valve2}}{A_{gap}} \sqrt{2\left(\dfrac{P_s}{\rho_s} - \dfrac{P_{gap}}{\rho_{gap}}\right)}}{\dfrac{L_{gap}}{\mu_{gap1}} + \dfrac{L_{core}}{\mu_{core}} - nk} - \frac{\dfrac{\rho_{gap} A_{gap}}{\rho_{atm} A_{valve3}} \sqrt{2\left(\dfrac{P_{gap}}{\rho_{gap}} - \dfrac{P_{atm}}{\rho_{atm}}\right)}}{\dfrac{L_{gap}}{\mu_{gap2}} + \dfrac{L_{core}}{\mu_{core}} - nk} \right). \tag{2.39}$$

The following simplification will help to reduce the complexity of this equation producing Equation (2.40):

- $\dfrac{P_{gap}}{\rho_{gap}} = \dfrac{P_{atm}}{\rho_{atm}}$ for Δt_{in},

- $\dfrac{P_{gap}}{\rho_{gap}} = \dfrac{P_s}{\rho_s}$ for Δt_{out} and $V_{gap} << V_s$,

- $\rho_{atm} \approx 1$, and

- $A = h_g w_g$.

To allow a full theoretical analysis the following substitution, $v_{gas} = \sqrt{2\left(\dfrac{P_s}{\rho_s} - \dfrac{P_{atm}}{\rho_{atm}}\right)}$, is

made,

$$V = \mu_o n H_m L_m w_g v_{gas} \left(\frac{\dfrac{A_{valve2}}{A_{gap}}}{\dfrac{L_{gap}}{\mu_{gap1}} + \dfrac{L_{core}}{\mu_{core}} - k} - \frac{\dfrac{\rho_s A_{gap}}{A_{valve3}}}{\dfrac{L_{gap}}{\mu_{gap2}} + \dfrac{L_{core}}{\mu_{core}} - k} \right). \qquad (2.40)$$

The electrical energy output of the magnetic fuel cell is

$$\Delta E_{cycle} = \frac{V^2}{R} t_{cycle}, \qquad (2.41)$$

where ΔE_{cycle} is electrical energy produced by the magnetic fuel cell each cycle, and R is load resistance. The power of the magnetic fuel cell is

$$P_{cell} = \frac{V^2}{R}, \qquad (2.42)$$

where P_{cell} is the power produced by the magnetic fuel cell each cycle.

To determine efficiency, first an energy balance will be used to balance the energy removed from the gas to the energy produced by the fuel cell (assuming no losses),

$$V_{gap} \Delta P_{mag} = \Delta E_{cycle}. \qquad (2.43)$$

This becomes

$$\Delta P_{mag} = \frac{V^2 t_{cycle}}{R V_{gap}}, \qquad (2.44)$$

where ΔP_{mag} is the magnetic pressure drop caused by the magnetic fuel cell, and V_{gap} is the volume of the gap. The efficiency is derived by using the energy of the fuel cell divided by the total energy of the gas,

$$\varepsilon = \frac{\Delta E_{cell}}{\Delta E_{total}}, \qquad (2.45)$$

$$\varepsilon = \frac{\frac{V^2}{R} t_d}{P_s V_s - P_{atm}(V_s + V_{gap})}, \quad (2.46)$$

where:

- ε, efficiency of the magnetic fuel cell,

- ΔE_{total}, total energy of the gas, and

- ΔE_{cell}, total energy of the magnetic fuel cell.

The efficiency equation can be simplified by assuming,

$$P_s V_s \gg P_{atm}(V_s + V_{gap}), \quad (2.47)$$

therefore ,

$$\varepsilon = \frac{V^2 t_d}{R P_s V_s}. \quad (2.48)$$

Several substitutions can be made shown below:

- substitute in duration time,

$$\varepsilon = \frac{V^2}{R P_s \dot{V}_{cycle}}, \quad (2.49)$$

- substitute in volume flow rate,

$$\varepsilon = \frac{V^2 t_{cycle}}{R P_s V_{gap}}, \quad (2.50)$$

- substituting into Equation (2.50), the effect of magnetic pressure,

$$\varepsilon = \frac{V^2 t_{cycle}}{R(P_s - \Delta P_{mag})V_{gap}} = \frac{V^2 t_{cycle}}{R\left(P_s - \frac{V^2 t_{cycle}}{R V_{gap}}\right)V_{gap}} = \frac{1}{\left(\frac{R P_s V_{gap}}{V^2 t_{cycle}} - 1\right)}, \quad (2.51)$$

- substitute in voltage,

$$\varepsilon = \frac{t_{cycle}}{RP_s V_{gap}}\left(\mu_o n H_m L_m w_g v_{gas}\left(\frac{\frac{A_{valve2}}{A_{gap}}}{\frac{L_{gap}}{\mu_{gap1}}+\frac{L_{core}}{\mu_{core}}-k}-\frac{\frac{\rho_s A_{gap}}{A_{valve3}}}{\frac{L_{gap}}{\mu_{gap2}}+\frac{L_{core}}{\mu_{core}}-k}\right)\right)^2 , \quad (2.52)$$

- substitute in volume of gap,

$$V_{gap} = w_{gap} h_{gap} L_{gap} , \quad (2.53)$$

$$\varepsilon = \frac{w_{gap} t_{cycle}}{RP_s h_{gap} L_{gap}}\left(\mu_o n H_m L_m v_{gas}\left(\frac{\frac{A_{valve2}}{A_{gap}}}{\frac{L_{gap}}{\mu_{gap1}}+\frac{L_{core}}{\mu_{core}}-k}-\frac{\frac{\rho_s A_{gap}}{A_{valve3}}}{\frac{L_{gap}}{\mu_{gap2}}+\frac{L_{core}}{\mu_{core}}-k}\right)\right)^2 .(2.54)$$

From Equation (2.54), several observations can be made. The magnetic permeability of free space, μ_o, times the magnetic field strength, H_m of the magnet is approximately one. The number of turns variable, n, is squared but there is an implicit relationship between n and load resistance, R. The impact of this is that maximizing n will also raise resistance R when trying to maximize power transfer. This will be discussed in detail in Section B. The magnetic terms under the denominator in Equation (2.54), $\left(L_{core}/\mu_{core}\right)-k$, are the same for both denominators with the exception of the permeability of the gap terms, μ_{gap1} and μ_{gap2}. Therefore, to maximize voltage and efficiency both the core length divided by the core permeability, $\left(L_{core}/\mu_{core}\right)-k$, and the k term should be minimized using a large core permeability value, μ_{core}. The velocity of the gas, v_{gas} also has a dependent relationship between itself and supply tank pressure, P_s; the consequence being, minimizing supply tank pressure also minimizes gas velocity. The rest of the terms reveal order of magnitude effects on efficiency based upon their relative magnitude and are listed in Equations,(2.55)-(2.59), below, in order of decreasing importance:

$$\varepsilon \propto \frac{1}{L_{gap}^3} , \quad (2.55)$$

$$\varepsilon \propto L_m^2 , \quad (2.56)$$

32

$$\varepsilon \propto w_{gap}, \tag{2.57}$$

$$\varepsilon \approx t_{cycle} \text{ and} \tag{2.58}$$

$$\varepsilon \approx \frac{1}{h_{gap}} . \tag{2.59}$$

B.   RESISTANCE ESTIMATION AND COIL OPTIMIZATION

The number of windings term, n, in Faraday's Induction Equation, (2.34), is a key parameter effecting coil optimization. On the surface, a larger number of windings should generate a large voltage output (Equation (2.34)). But, looking at power produced by the fuel cell shows that internal resistance and therefore load resistance also increases as number of windings increases (Equation(2.60)). Increasing the number of windings causes the internal current to drop and therefore output power to drop. This Section optimizes the power factor term, n^2 / R, in the power equation with respect to winding resistance, since

$$v = -n\frac{\Delta\phi}{\Delta t} \rightarrow P = \frac{v^2}{R} \rightarrow P \propto \frac{n^2}{R} . \tag{2.60}$$

In order to establish equivalency between two different gauge size wires, a fixed winding cross-section is used (refer to Figure 6) with the horizontal distance represented as x and the vertical distance represented as y. This analysis is based upon two simplifying assumptions, one being the wire is wound around a circular magnetic core with radius, a, and the other being the wire itself is circular with radius, b.
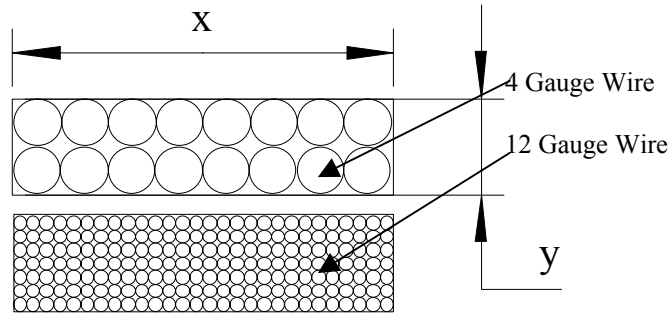
Figure 6   Two Examples of Wire Winding Cross-Sections.

The number of windings fitting onto each layer, n_{layer}, of the coil can be determined using geometry,

33

$$n_{layer} = \frac{x}{\text{wire diameter}} = \frac{x}{2b}. \tag{2.61}$$

The total number of layers, n_y, is then determined as

$$n_y = \frac{y}{2b}. \tag{2.62}$$

The total number of windings, n, is

$$n = n_{layer}n_y = \frac{xy}{4b^2}. \tag{2.63}$$

The length of the first layer, $L_{layer\,1}$, is determined using

$$L_{layer\,1} = (\text{loop circumference})\, n_{layer} = 2\pi a n_{layer} \tag{2.64}$$

The length of the second layer, $L_{layer\,2}$, is found as

$$L_{layer\,2} = 2\pi(a+2b)n_{layer}. \tag{2.65}$$

The total length of the coil, L_{coil}, accounting for all layers is

$$L_{coil} = 2\pi n_{layer} \sum_{k=1}^{k=n_y}\left(a+2b(k-1)\right). \tag{2.66}$$

Substituting in Equations (2.61) and (2.62) in Equation (2.66) produces

$$L_{coil} = \pi \frac{x}{b} \sum_{k=1}^{k=\frac{y}{2b}}\left(a+2b(k-1)\right). \tag{2.67}$$

The equation for resistance of a wire [10] is given by

$$R = \frac{\rho_w L_{coil}}{A_{wire}}, \tag{2.68}$$

where:

- ρ_w is the resistivity of the wire,

- L_{coil} is the total length of the coil, and

34

- A_{wire} is the cross sectional area of the wire.

Substituting Equation (2.67) into Equation (2.68) produces

$$R = \frac{\rho \pi x}{\pi b^3} \sum_{k=1}^{k=\frac{y}{2b}} \left(a + 2b(k-1) \right).$$
(2.69)

Finally, substituting, Equations (2.63) and (2.69) back into the power factor constant, Equation (2.60), produces (normalizing $x, y = 1$)

$$\frac{n^2}{R} = \frac{1}{16\rho b \sum_{k=1}^{k=\frac{1}{2b}} \left(a + 2b(k-1) \right)}.$$
(2.70)

Equation (2.70) is plotted in Figure 7 with a varied wire cross-section, b, and a fixed loop radius, $a = 0.1025 \text{ m}$. This plot shows that changes in the wire cross-section are almost linearly compensated for by the summation. Therefore, to maximize the power factor constant in Equation (2.70), minimize the loop radius, a. Equation (2.70) can be simplified to

$$\frac{n^2}{R} \approx \frac{1}{a}.$$
(2.71)
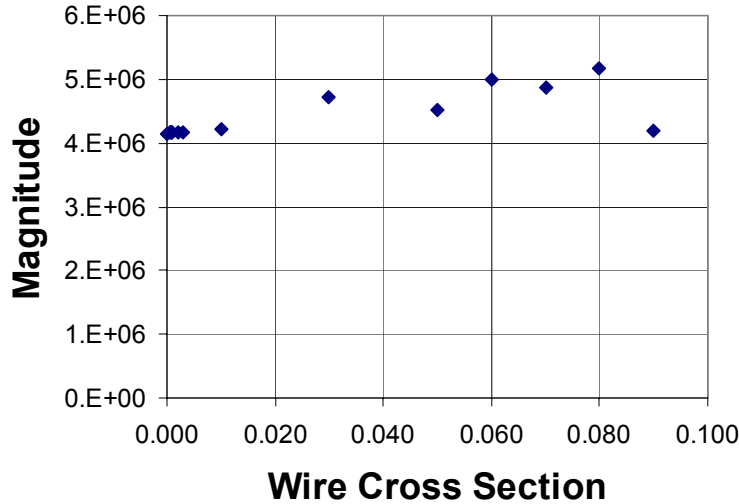
Figure 7   Plot of Power Factor Constant for Varying Wire Cross-Sections.

Using actual wire gauge sizes, a plot of power versus number of windings is shown in Figure 8. Faraday's Induction law, Equation (2.72), was used to build Figure 8. The change in magnetic flux was 10^{-5} T. The area was 0.02 m^2. The change in time was 10^{-3} s. The resulting equation was then found to be,

$$P = \frac{V^2}{R} = \frac{1}{R}\left(\frac{n\Delta BA}{\Delta t}\right)^2 = \frac{n^2}{R}\left(\frac{1 \times 0.02}{10^{-3}}\right)^2 = \frac{400n^2}{R},$$ (2.72)

where R is a function of n. Figure 8 shows there are an optimal number of windings to achieve maximum power. This plot also shows that lower gauge wires produce a larger power output even though they have less windings. The theory for the magnetic fuel cell is now applied to the experimental setup.
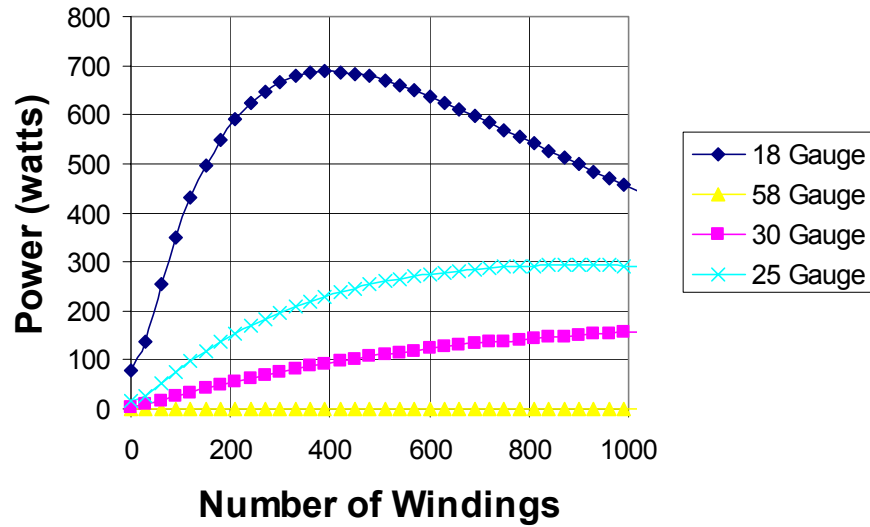
Figure 8   Power vs. Number of Windings for Different Gauge Wires.

C.   IMPLEMENTATION

1.   Configuration Decision

The equipment determination for the experiment was based upon low-cost commercial components. The pressure of 2000 psi used in the experiment was based upon the smallest high-pressure sample chamber offered by Sunnyvale Valve and Fitting Company [11]. The smallest chamber was also chosen to minimize the length of the gap. The smallest chamber diameter was two inches. The quarter-inch copper tubing was

36

chosen based upon being already available on site. This dictated the sample chamber and valve inner diameter sizes as one-quarter inch.

The permanent magnets were obtained from Stanford Magnetics Corporation [12]. Nd-B-Fe-40 magnets having a very high residual magnetic field and high coercivity are sold at a low cost. The number and size of the magnets were chosen based upon the height and diameter of the sample chamber (i.e., eight inches by two inches). A holding apparatus for the magnets was designed and fabricated by George Jaksha, the NPS physics department machinist. This apparatus held the permenant magnets against the sample chamber and maintained alignment with respect to each other. An air-gap magnetic return path was chosen over a soft magnetic material core path due to excessive costs of the soft magnetic materials.

Due to the high-speed high-pressure requirements of the valves, Swagelock ball valves were chosen to provide quick operation in both opening and closing. Twenty-four gauge wire was chosen for the magnetic fuel cell coil due to it being available on site and in large quantity. This wire allowed a large number of windings to be wrapped around the sample chamber support apparatus.

2.   Experiment Predictions

With the material geometries established, the predicted quantities of the experiment can be determined. This experiment, being the first of its kind, focused on obtaining an output voltage from the fuel cell. Only the discharge portion of the fuel cell cycle is developed since this theoretically should produce the largest voltage. The derivation is shown in Appendix C. The input values and constants are summarized in Table 2 of Appendix D. All the derived values are shown in Table 3 of Appendix D. For this configuration, the predicted voltage to be sensed was –2.75 millivolts to occur in roughly 3.66 milliseconds.

This chapter performed an indepth analysis of the theory of the magnetic fuel cell. A brief discussion was provided on optimizing the number of windings of the magnetic fuel cell coil. Several experimental design decisions were discussed along with the predicted voltage response of the experiment. Having determined the theoretical

characteristics of the magnetic fuel cell, Chapter IV discusses the experimental setup and implementation of the experiment.

IV. EXPERIMENT

A. OVERVIEW

The experiment was conducted in the Rail Gun Lab in Spanagel Hall at the Naval Postgraduate School in November of 2002. The goal of the experiment was to verify theoretical equations and predictions developed in Chapter III.

The magnetic fuel cell is shown in Figure 9. The picture on the left is without the coil and the picture on the right is with the coil. In the picture without the coil, the gray structure wrapped with tygon tubing is the support apparatus mentioned in Chapter III. Four wood inserts were provided for additional support. The gas tubing with connectors can be seen on either end of the pressure chamber, which is located inside the support apparatus. The picture on the right of Figure 9 is the fuel cell with 515 windings of 25-gauge wire wrapped around it. Duct tape was used to ensure the windings stayed tightly wound around the support apparatus.
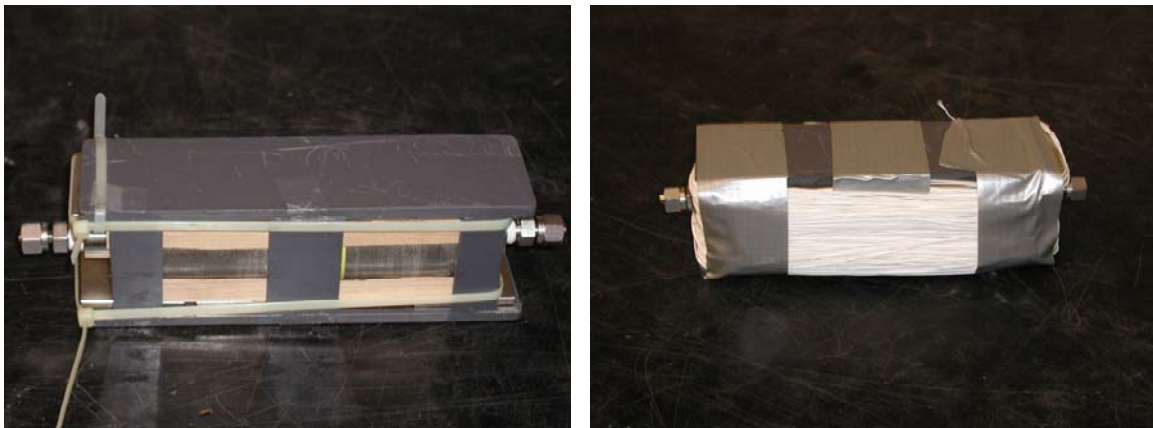
Figure 9   Magnetic Fuel Cell: (left) without coil, (right) with coil.

B. SETUP

A diagram of the experimental setup is shown in Figure 10. Nitrogen and air were the diamagnetic and paramagnetic gases used. An oscilloscope was used to determine output voltage. An open microphone was used to provide an audio trigger caused by the vibration noise. There was considerable vibration noise developed by the magnetic fuel cell due to the rapid expansion of 2000-psi gas to atmospheric pressure.
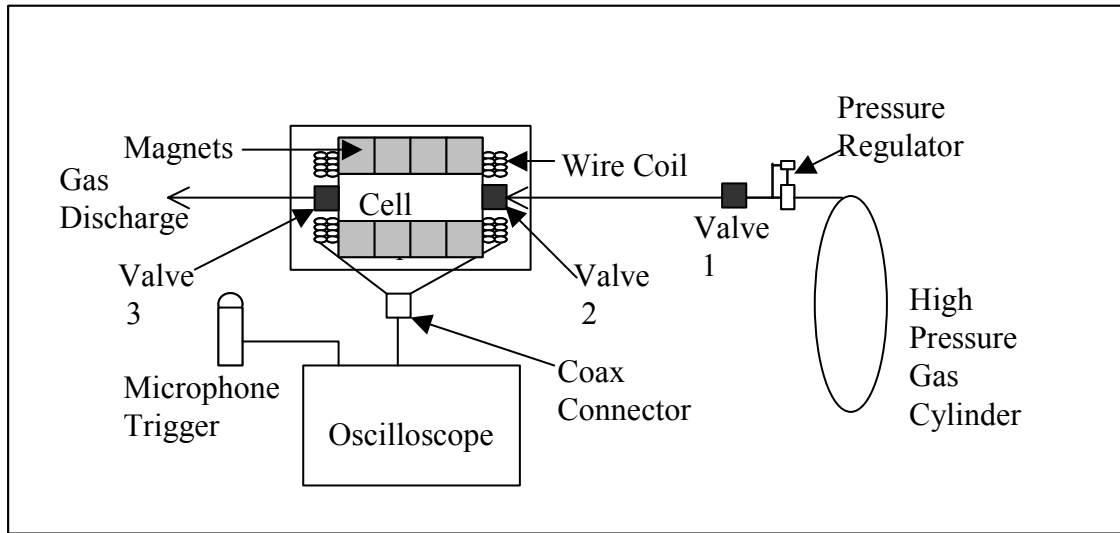
Figure 10   Schematic of Test Setup.

1.   Equipment

Eight two-inch by two-inch by one-quarter-inch Nd-B-Fe-40 magnets were used in the experiment to magnetize the paramagnetic gas. The magnets characteristics are listed in Table 1. An explanation of each term is provided below.

- The residual inductance, B_r, is the value of induction at the point of the hysteresis loop, at which the hysteresis loop crosses the B axis at zero magnetizing force. The B_r represents the maximum magnetic flux density output of the magnet without an external magnetic field.

- The coercivity of the magnet, H_C, is the demagnetizing force, measured in Oersted, necessary to reduce observed induction, B to zero after the magnet has previously been brought to saturation.

- The intrinsic coercivity, H_{ci}, is an intrinsic ability of a magnet to resist demagnetization. Its value is measured in Oersted and corresponds to zero intrinsic induction in the magnet after saturation.

- The $(BH)_{max}$ term which is a representation of the overall energy of the magnet. There is a point on the hysteresis loop at which the product of magnetizing force H and induction B reaches a maximum. The maximum value is called the Maximum Energy Product. At this point, the volume of magnet material required to project a given energy into its surrounding is a

40

minimum. This parameter is generally used to describe the "strength" of the permanent magnet material.

- The Curie temperature is the temperature at which the parallel alignment of elementary magnetic fields completely disappears and the material is no longer able to hold magnetization.

- The maximum operating temperature is the temperature above which the magnets will start demagnetizing.

Table 1.   Magnetic Characteristics of Nd-B-Fe-40 (after [12]).

Grade	B_r (KG)	H_C (KOe)	H_{ci} (KOe)	$(BH)_{max}$ (MGOe)	Curie Temp. (^{o}C)	Max. Op. Temp. (^{o}C)
N40	12.5-12.8	>11.6	>12	38-41	310	80

Five hundred 24-gauge copper windings were wound around the pressure chamber to detect the magnetic field change caused by the pressurized gas. The gas cylinder containing 2000 psi was used as the gas source for the experiment. A 5600B series high-pressure regulator regulated downstream gas pressure to 1800 psi. All three valves used in the system were high-pressure rated, one-quarter-inch, Swagelock "40" series ball valves [11].

Valve one acted as a two-valve isolation between the high-pressure tank and downstream piping. Valve two controlled gas flow into the cell gap and isolated the gap from upstream pressure when valve three was opened. Valve three isolated the gap from atmosphere when valve two was open. (Ideally, an automated system using solenoid-operated valves would charge and discharge the cell gap at a user-controlled frequency.)

The pressurized chamber containing a two-inch cell gap is a Swagelock 316L stainless steel sample cylinder with an eight-inch length and a one-quarter inch cell wall rated for 5000 psi [11]. Both valves and sample chamber were chosen to be stainless steel 316L due to this material's anti-ferromagnetic properties and ability to handle high-pressures. The piping between the regulator and valve one is one-quarter inch copper tubing. The piping between valves one and two was 7000 psi rated flexible tubing. Valve three vented the high-pressure gas in the gap to atmosphere.

The eight magnets are held in place against the sample chamber by a fabricated PVC cubic container with rounded wood wedges in the corners (Figure 11). Figure 11

shows a cutout cross-section of the magnetic fuel cell with dimensions. A Radio Shack omni-microphone was used to trigger the scope on discharge of the gas. The windings and the oscilloscope were connected by a coaxial cable.
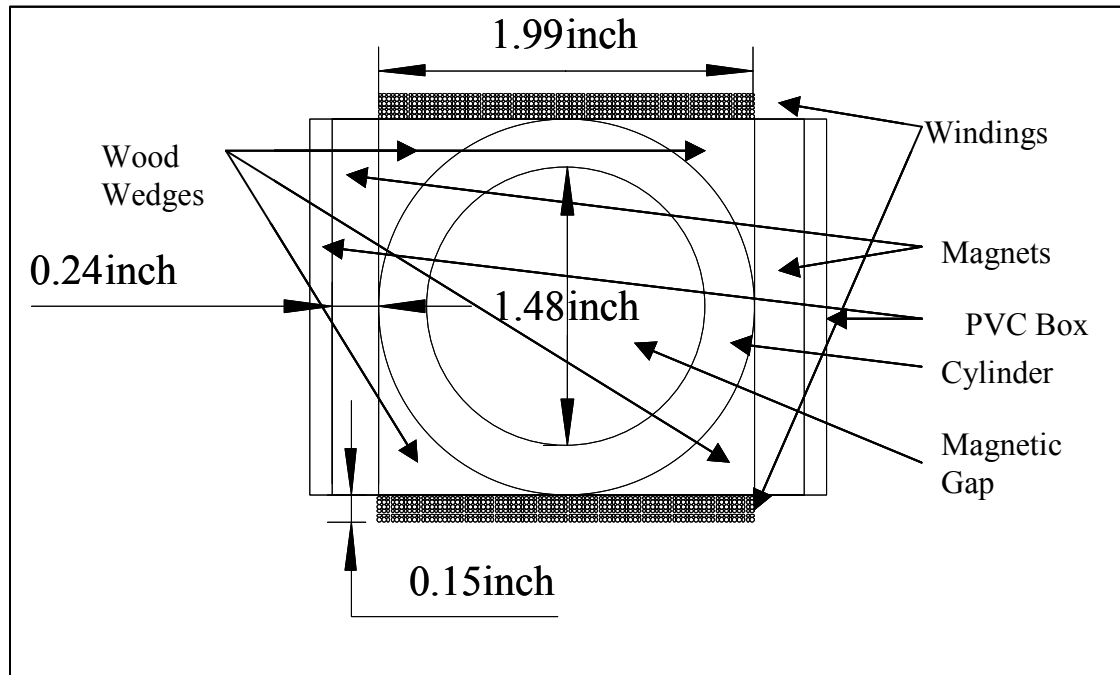
Figure 11   Cross Section of Fuel Cell.

2.   Calibration

A Hall-effect Gauss-meter was used to determine the magnetic field within the de-pressurized cylinder. At the center-point of the cylinder with the probe extending in four inches, the magnetic field was measured to be 0.1 Tesla. This agreed with the predicted value of 0.1 Tesla derived in Appendix D. To verify operation of the outer coil and determine the coupling parameter of the circuit, the following PSPICE test circuit was simulated (Figure 12). A seven-coil wire loop was made from 24-gauge insulated copper wire and inserted inside the pressure chamber. A high current voltage source and high power IGBT (Figure 13) was used in parallel with a square wave generator and a voltage source. The IGBT was triggered off a square wave pulse source with a pulse width of 30 milliseconds. The rise time on the pulse was nine microseconds. A current pulse of two amps was applied to the loop. The output of both the pulse source and fuel cell windings was connected to channels one and two of the oscilloscope.
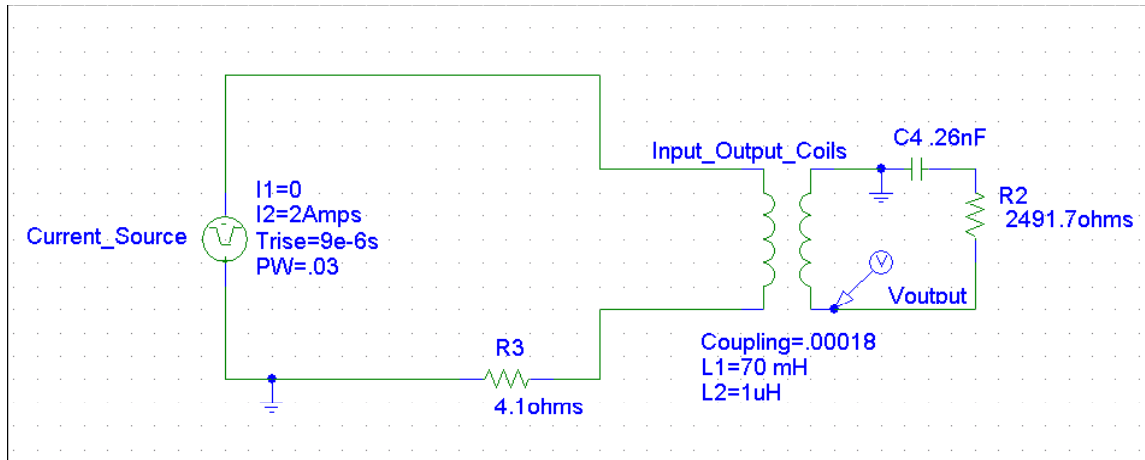
Figure 12   PSPICE Model of Calibration Signal From Test Coil.

Figure 13   Voltage Source and High Power IGBT.

Both the test signal and PSPICE model output are shown in Figure 14 and Figure 15. A significant effort was made to get the test signal output of the oscilloscope and the PSPICE model output to match. The test coil and fuel cell coil were measured for inductance. The test signal in Figure 14 provided the necessary data to model the signal in PSPICE and determine the magnetic coupling loss of the circuit. The peak voltage output was 16.4 millivolts in both figures. The signal was a dampened sinusoid. The following discussion compares the PSPICE simulation to the measured calibration output.
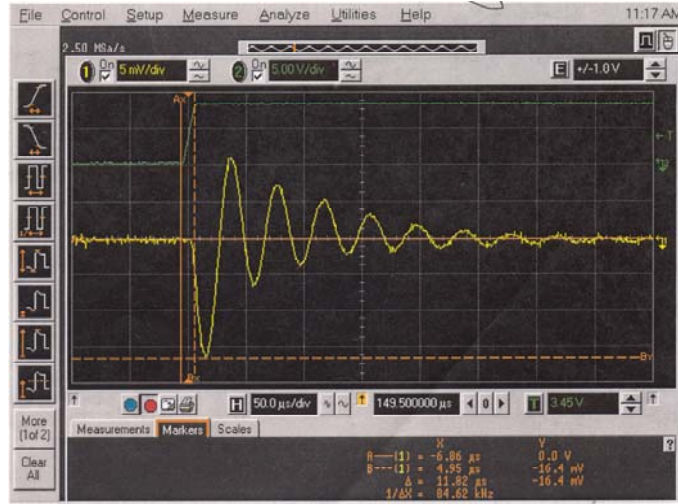
Figure 14 Oscilloscope Screen Capture of Input/Output Waveforms (Test Coil Inside Pressure Chamber).
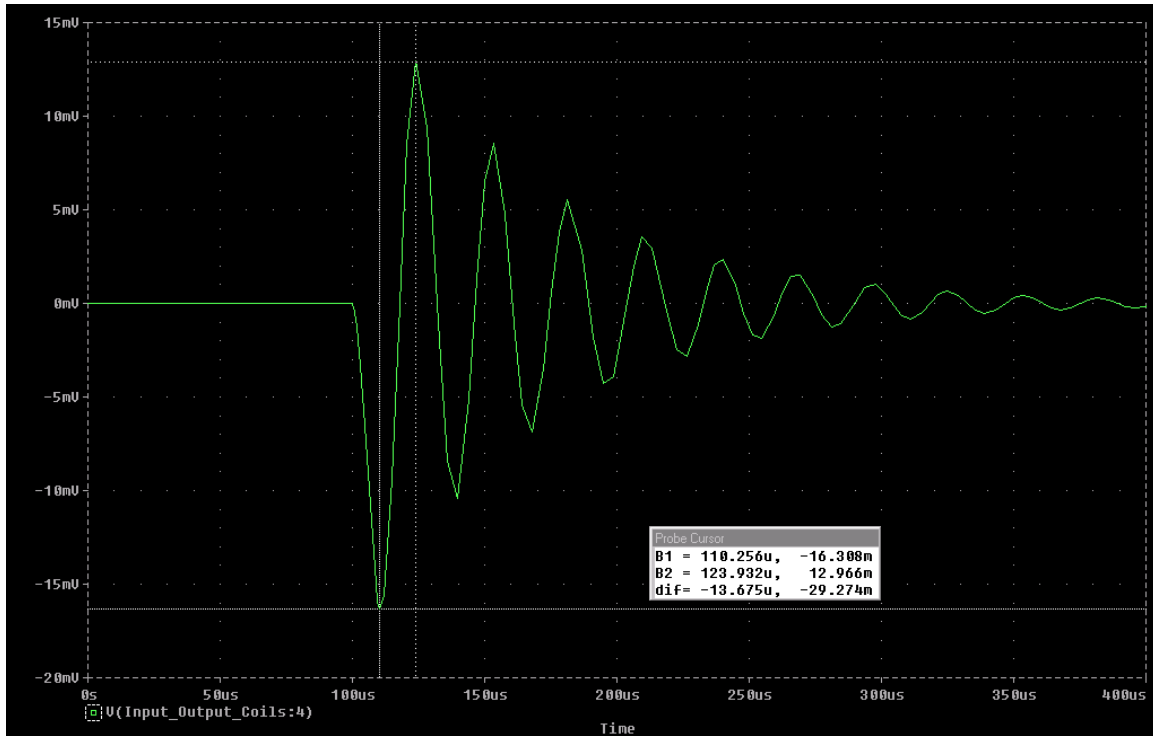
Figure 15 PSPICE Model of Calibration Signal (Test Coil Inside Pressure Chamber).

Knowing the resistance of the internal coil was $R = 0.02\ \Omega$, the following equation was used to determine the PSPICE parameters,

$$I(t) = I_o e^{-\frac{tR_e}{L}},\qquad\qquad(3.1)$$

44

where:

- $I(t)$ is the output current with respect to time,

- I_o is the initial current at time zero,

- R_e is the effective resistance of the circuit,

- L is the inductance of the test coil, and

- t is the time.

The first step determined the capacitance, C. This was accomplished by using the resonant frequency, $f = 42.3\,\text{kHz}$, from Figure 14 and applying to the resonant frequency equation to determine the capacitance,

$$f = \frac{1}{2\pi\sqrt{LC}} \rightarrow C = \frac{1}{(2\pi f)^2 L} = 0.26\text{pF}. \tag{3.2}$$

The second step determined the current, I_{pk-1}, at the first voltage peak in Figure 14, where $V_{pk-1} = 16.4$ millivolts,

$$I_{pk-1} = \frac{V_{pk-1}}{R} = 0.82\ \text{A}. \tag{3.3}$$

The third step determined the current at the next peak, I_{pk-2},

$$I_{pk-2} = \frac{V_{pk-2}}{R} = 0.55\ \text{A}. \tag{3.4}$$

The time difference between peaks was $\Delta t_{peaks} = 11.22\ \mu\text{s}$. Equation (3.1) can be rearranged to determine the effective resistance of the combined two-coil pair, $R_e = 2491.7\,\Omega$. The resistor, $R4$, shown in Figure 12 was determined by adjusting its value to make the output of the primary coil equal to the experimental value of 8.5 volts.

The only variable unknown in the PSPICE model was the coupling factor. The coupling factor was iteratively solved for using the PSPICE model. This was done by comparing expected output of Figure 14 to the PSPICE model and resetting the coupling factor until a match of signals was achieved. The coupling factor, k_c, was found to be 0.00018. The importance of the coupling factor is based upon the test coil configuration.

The test coil had to be inserted through a one-quarter inch diameter opening on the end of the pressure chamber. The geometry of the test coil was a rectangle with a length of seven inches and width of ¾ of an inch. (The resulting area, A_{test}, was 5.25 square inches.) The sample chamber had an area, $A_{chamber}$, of 13.6 square inches. The fuel cell's magnetic cross-section area, A_m, was 16 square inches. The expected coupling factor for the test coil, k_c, was found by dividing the smaller area by the larger area,

$$k_c = \frac{A_{test}}{A_m} = 0.328.$$
(3.5)

The expected coupling factor between the sample chamber and fuel cell was, $k_c = 0.85$.

The large difference between the theoretical coupling factor and that found in PSPICE led to a second calibration test with the coil wound two times around the actual fuel cell windings. This should have made the coupling factor equal to one. Figure 16 shows the voltage input signal at 8.5 volts and voltage output signal's first peak at 1 volt. The actual signal output is shown in Figure 17. The output signal's first peak voltage was 1 volt and the coupling factor from the PSPICE model was 0.012. This coupling factor was then used to normalize the coupling factor found for the coil inside the chamber. The result was a coupling factor of 0.15. These results provide a margin of error for the predicted values of the fuel cell experiments with a range of $0.15 \leq V_{out} \leq 0.85$ to account for coupling factor.
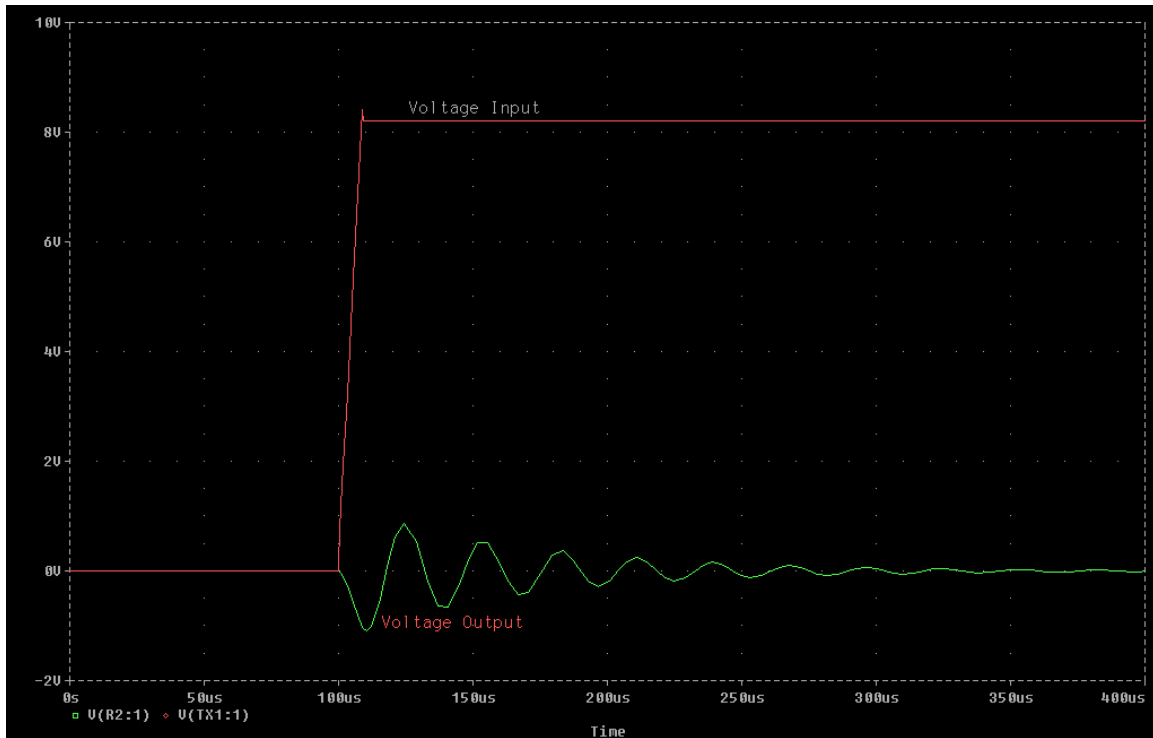
Figure 16   PSPICE Model of Calibration Signal (Test Coil Outside Pressure Chamber).
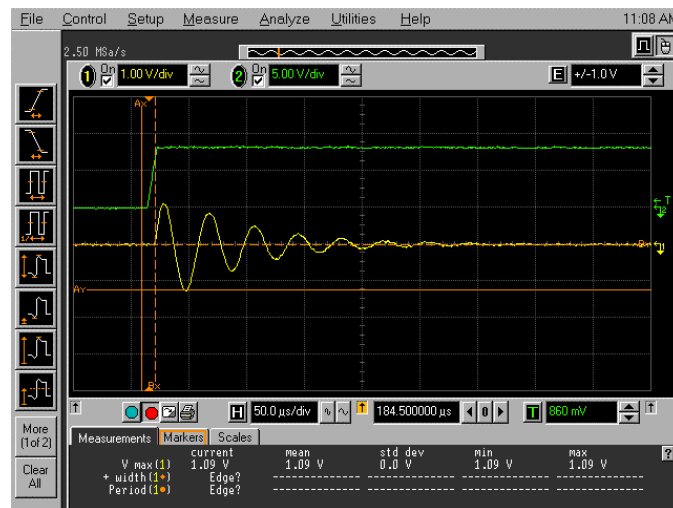
Figure 17   Oscilloscope Screen Capture of Input/Output Waveforms (Test Coil Outside Pressure Chamber).

The complete lab setup is shown in Figure 18. The HP oscilloscope is in the foreground with the yellow air bottle on the right. The round metallic cylinder was used to diminish the discharge blast, and the sandbags were used to help reduce mechanical vibration. The signal generator on the left of Figure 18.

Figure 18   Experiment.

3.   Operation

A stable 0.1 Tesla magnetic field was generated using four permanent magnets situated on each side of a stainless steel cylinder. A Hall-effect Gauss-meter verified the static magnetic field in the gap at atmospheric pressure was 0.1 Tesla agreeing with the calculation and modeling (the modeling predicted 0.1 Tesla). A 22-gauge wire coil with 515 turns was placed around the sample cylinder to sense magnetic flux changes. Air at 1800 psi was pulsed into the sample cylinder using valve two. The gas enhances the lines of flux within the gap causing a voltage to be induced in the coil. The gas then exits the cylinder causing the lines of flux in the gap to decrease. This flux decrease causes an opposite polarity voltage to be induced in the coils. The coil is connected to a HP INFINIUM 400 MHz oscilloscope (Figure 19), which measured the output voltage.
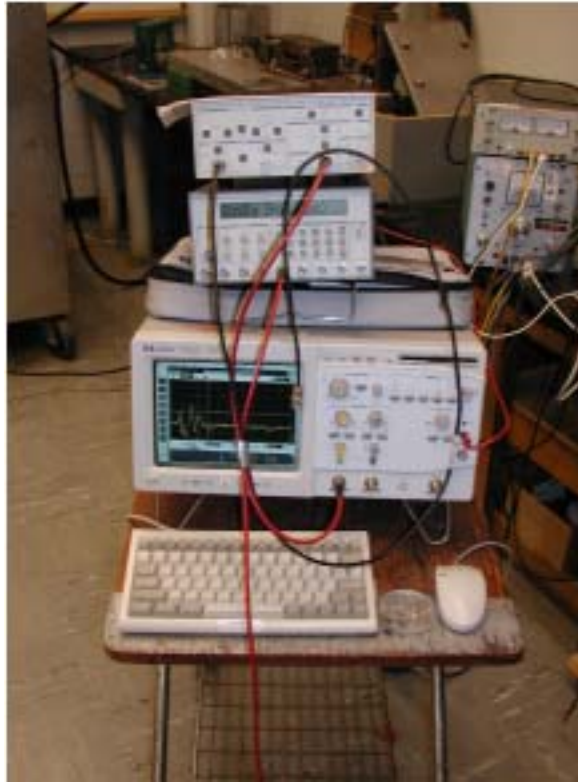
Figure 19   HP INFINIUM 400 MHz Oscilloscope.

The microphone connected to the oscilloscope trigger function, activated upon receiving an un-amplified signal of 10 millivolts. The noise burst lasts for approximately 200 milliseconds.

C.   EXPERIMENTAL RESULTS

The output of the magnetic fuel cell is shown in Figure 20. The peak voltage was 6.3 millivolts and lasted for 0.3 milliseconds. The expected voltage was 2.8 millivolts for a duration of 3.6 milliseconds (from Appendix D). The measured voltage was 2.3 times greater than expected while the signal duration was one tenth of the expected value.
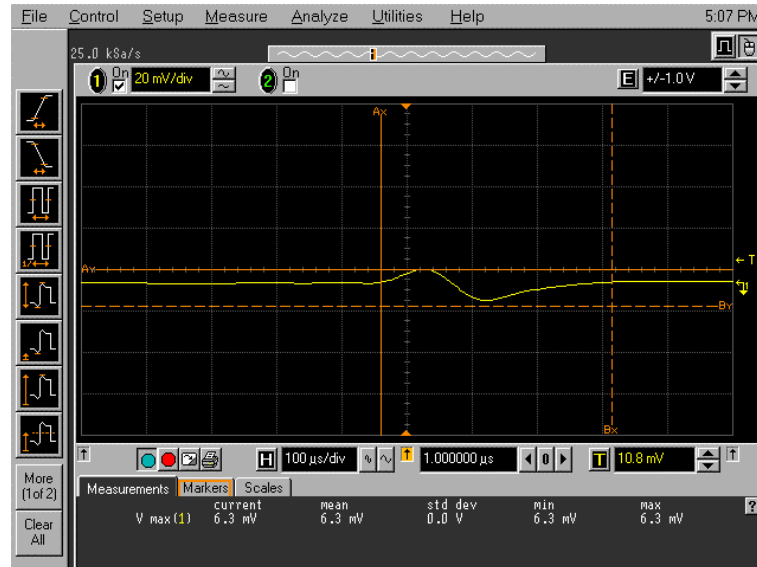
Figure 20   HP Oscilloscope Screen Capture of Magnetic Fuel Cell Output using
Compressed Air.

Figure 21 shows the theoretical voltage values versus the predicted gas output time (blue
line). The predicted voltage spans three orders of magnitude over ten milliseconds. The
theoretical derivation showed a discharge time of 3.6 milliseconds (red square). The
manufacturer of the one-quarter-inch valves [11] established a time of 0.5 millisecond for
the gas to exit the pressure chamber at 1800 psi (blue triangle with the voltage set to the
measured value of 6.3 millivolts). The actual voltage and time were 6.3 millivolts and
0.3 milliseconds (green circle). The experimental results demonstrate the challenge in the
analysis. A small difference in the expected time for the gas to exit causes the output
voltage to change considerably.
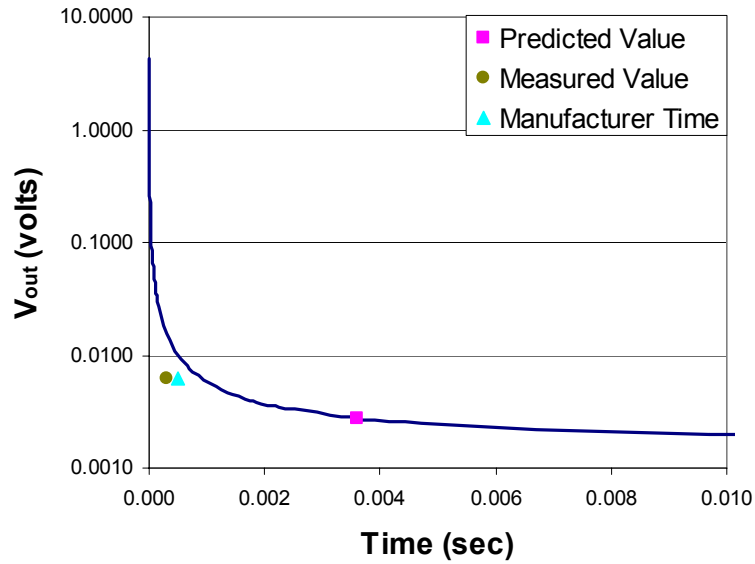
Figure 21   Voltage Output vs. Change in Time Out.

The predicted voltage varies linearly with pressure as shown in Figure 22 (blue line). The voltage output with respect to pressure was very stable and easy to predict. The measured value (green triangle) was within a factor of two of the predicted value (red square).
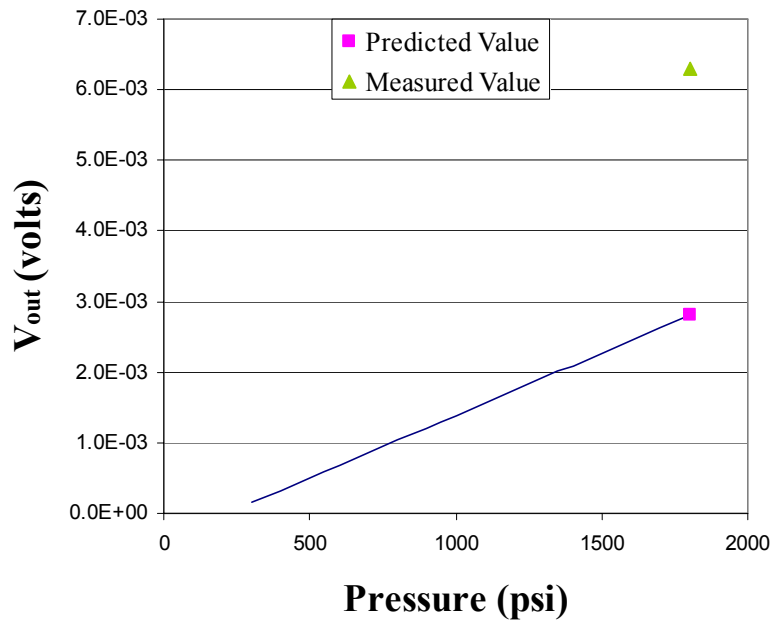
Figure 22   Plot of Predicted Voltage vs. Supply Pressure.

One challenge that became clear early on in the experimentation was properly triggering the scope. The vibration audio signal created by the rapid depressurization of the air in the pressure chamber was used to trigger the scope. The vibration additionally induced a voltage signal from movement of the coil. The rapid expansion of the gas out of the chamber caused the magnets to vibrate for a period of 200 milliseconds. A reduction of the vibration noise magnitude was finally achieved by tightly wrapping the magnetic fuel cell with tygon tubing and placing several 20-pound sandbags on top of it.

Bernoulli's principle was adapted from its true purpose of modeling fluid flows to determine timing of the gas, Δt_{out}. This adaptation and the mechanical vibration prevented an accurate measurement of Δt_{out}. The initial experiments were obtaining approximately 15-millivolt vibration pulse signals shown in Figure 23. This was later reduced with tygon tubing and sand bag modifications mentioned above.

Figure 23   HP Oscilloscope Screen Capture of Vibration Caused Noise Output.

The next section discusses the knowledge learned from this experimental setup.

D.   LESSONS LEARNED

The next experimental model should incorporate the following improvements to its configuration.

- Reduce the magnetic gap and height to optimize magnetic field strength in the gap and reduce the air volume required to change the magnetic field.

- Use a high frequency soft magnetic core as the magnetic return path to decrease magnetic coupling losses and allow the coil to be moved from the gap to the core.

- Use 10-14 gauge wires as the windings to optimize the power factor term and thus optimize fuel cell power output.

- Electro-magnetically isolate the entire fuel cell system and permanently pot the fuel cell to minimize mechanical vibration.

- A software-modeling program such as FEMLAB for MATLAB [13] may be useful. This program allows multi-physics modeling and is very intuitive.

- Use flexible pressure hoses vice copper tubing as input to the fuel cell to reduce mechanical vibration.

- Keep the size of the valves and piping larger than the cross-sectional area of the pressure chamber to maximize gas flow.

- Find solenoid-operated high-pressure valves to act as inlet and outlet to the fuel cell. (This will allow better signal isolation and better characterizing of the fuel cell.)

- Re-examine Bernoulli's Principle and its application to the fuel cell to better isolate timing performance.

- Purchase a flow detector for the fuel cell.

Chapter IV discussed the setup, calibration and testing the magnetic fuel cell. Analysis of the test results showed a close agreement between the predicted and measured voltages and gas flow times. The final section of this chapter provided an extensive list of lessons learned and suggestions in designing the next magnetic fuel cell experiment. Chapter V provides a conclusion to the thesis, discussing what a next generation magnetic fuel cell is capable of and provides additional ramifications of the theory behind the magnetic fuel cell.

V.   CONCLUSION, OPTIMAL DESIGN AND RAMIFICATIONS

A.   CONCLUSION

This thesis discussed the development, design and testing of a magnetic fuel cell. The experiment showed the magnetic fuel cell produced a significant voltage output. The experiment provided insight to design a more advanced experiment. Two lessons learned were the importance of matching the magnetic circuit and the electrical circuit. An improperly matched magnetic circuit produced coupling losses. An improperly matched electrical circuit did not maximize the power transfer of the magnetic fuel cell. A future experiment should be designed to develop a larger power output and reduce the coupling and mechanical problems found in the first experiment. The next section will discuss the next generation design of the magnetic fuel cell.

B.   PROPOSED NEXT GENERATION DESIGN

Figure 24 shows the voltage output of the ideal magnetic fuel cell using solenoid operated charge and discharge valves operating at high frequency. The theoretical equations developed in Chapters II and III were used to design an optimized model. A 10,000-psi air supply tank with a storage capacity of 220 liters acted as the gas supply. The geometry of the magnetic fuel cell was a height of one millimeter and width of 50 millimeters using a soft magnetic core return path. The gap was 0.5 millimeters using two Nd-B-Fe-40 permanent magnets. The soft magnetic core used a 20-gauge coil with 10,000 windings. The voltage signal with a peak of ± 0.119 volts is a sinusoid operating at 1.6 Hz.
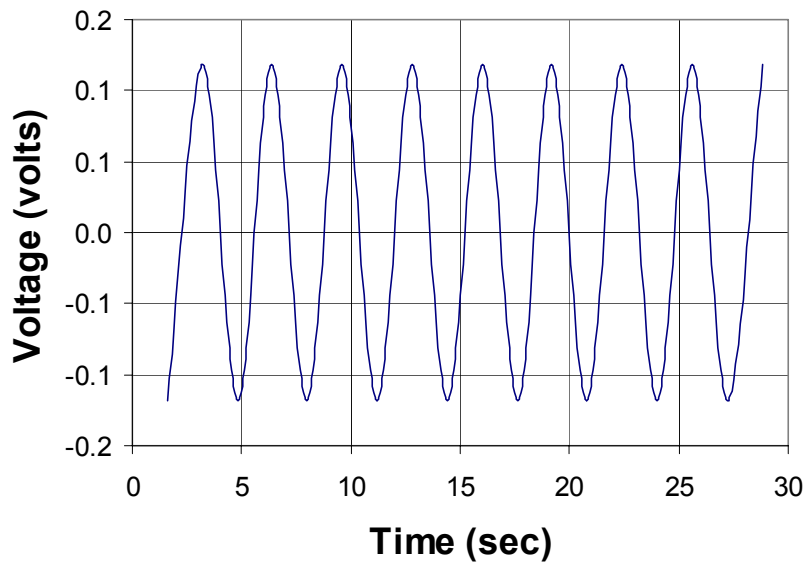
Figure 24   Voltage vs. Time for the Optimal Fuel Cell.

Figure 25 shows the fuel cell power versus duration time of the supply tank. This plot superimposes three values of gap width varying from 0.1 mm to 10 mm. To maximize power output the gap width should be made as large as possible.
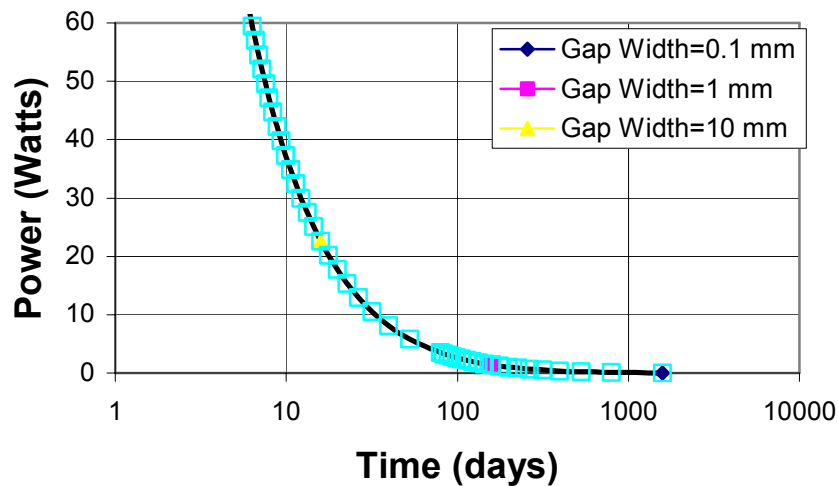
Figure 25   Optimal Fuel Cell: Power vs. Total Time (10,000 psi 220L tank).

Figure 26 shows efficiency as a function of fuel cell gap width for the fuel cell. Three gap widths are superimposed on the plot. A gap width of 0.1 mm produces the largest efficiency. This is in contrast to Figure 25 which showed a larger gap width is better. To optimize for both efficiency and power, a configuration having several fuel cells stacked

56

together would be optimal. This technique is already employed in hydrogen fuel cell systems [17].
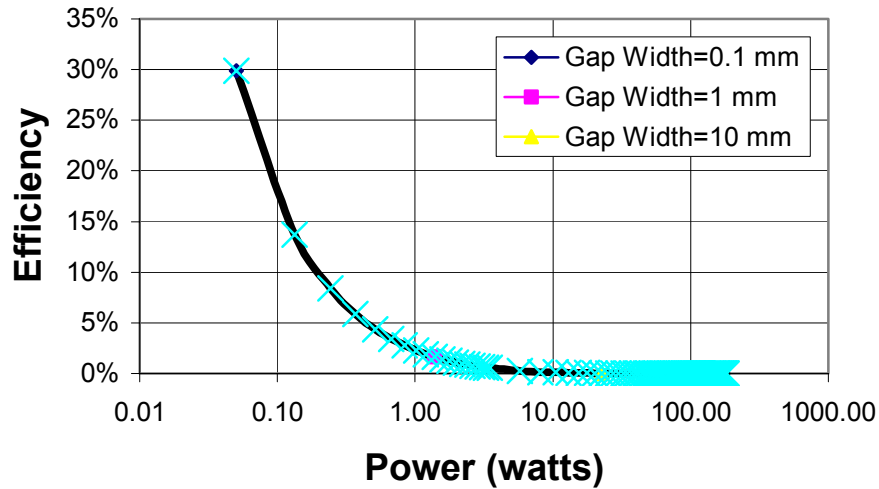
Figure 26   Optimal Fuel Cell: Efficiency vs. Power (10,000 psi 220L tank).

C.   RAMIFICATIONS

The theory developed in this thesis indicates several areas of research. Using the equations derived in Chapters II and III, it has become clear that it is feasible to construct an electromagnetic gas-flow control valve. Reducing the length of the gap of a magnetic fuel cell will increase the magnetic differential pressure (Equation (2.44)). With this configuration, it should be possible to raise the magnetic differential pressure higher than the gas pressure electronically; stopping gas flow. By reducing the magnetic differential pressure less than that of the gas pressure, the gas would flow at a reduced rate. This effect would throttle the gas flow. A throttle valve using a mechanical interface to slow or stop gas flow performs this function. Proper study of the magnetic pressure effect may provide a device that does not require a mechanical interface to control gas flow. A non-contact electromagnetic valve would be ideal in many applications where a mechanical interface is undesired or not feasible (e.g., high-pressure high-speed impulse jets). If this technology could be developed, it would have many applications both in the military and commercial industry. Such a electromagnetic valve would benefit the magnetic fuel cell development by replacing the solenoid-operated input and output valves. A similar approach has been realized in the form of a magnetic wind blower built by a group of Japanese researchers. They have shown that it is possible to produce wind using the

changing susceptibility of air and a high strength electromagnets in their research lab [14].

One avenue of optimization not discussed was that of optimizing the area term of Faraday's Induction Equation (Equation (1.24)). Since a sphere is the largest volume for a fixed surface area for any three-dimensional object, the magnetic fuel cell's optimal shape should be spherical. Area can be maximized while minimizing the number of windings, change in magnetic field and change in time.

The Earth is an example of a very large magnetic fuel cell. The voltage difference created by this magnetic fuel cell would be between the Earth's ground and the ionosphere. Richard Feynman discussed the mystery behind the energy in the ionosphere in his Feynman Lectures on Physics [15],

> Although the electric current-density in the air is only a few micromicroamperes per square meter, there are very many square meters in the earth's surface. The total electric current reach the earth's surface at any time is very nearly constant at 1800 amperes. This current, of course, is "positive" –it carries plus charges to earth. So we have a voltage supply of 400,000 volts with a current of 1800 amperes – a power of 700 megawatts!

> With such a large current coming down, the negative charge on earth should soon be discharged. In fact, it should take only a half an hour to discharge the entire earth. But the atmospheric electric field has already lasted more than a half-hour since its discovery. How is it maintained? What maintains the voltage? And between what and Earth? There are many questions. [15]

The earth's magnetic field acts as the magnetic source in this magnetic fuel cell model. The changes in air pressure caused by either heating or cooling in the earth's atmosphere would cause a voltage between the ionosphere and earth (Equation (1.37)). Alternatively, depending if the change in pressure is vertical or lateral, a potential difference between two laterally different air masses would be produced. Thus, the implication of the earth as a fuel cell provides a possible explanation of the origin of the electrical energy in the earth's ionosphere.

Finally, the magnetic fuel cell when optimized should provide a safe, inexpensive alternative to the hydrogen fuel cell and could be a replacement to batteries. Application of the magnetic fuel cell concept to energy storage and non-invasive gas flow detection

are two of many possible future developments. The magnetic fuel cell provides a safe, inexpensive, environmentally sound alternative to traditional portable energy systems and will act as a comparison benchmark for existent and future energy systems.

THIS PAGE INTENTIONALLY LEFT BLANK

APPENDIX A: FUEL CELLS

A fuel cell is an advanced power generation device developed to reduce the logistics, weight, cost, and size of traditional power sources. Alexander Grove invented an electric fuel cell in 1839 [16]. An electric fuel cell is a device that converts chemical energy into electrical energy directly. A hydrogen gas is directed down a proton exchange membrane, at the same time air flows in parallel to hydrogen down an opposing membrane. In between the two membranes, an electrolyte transports the proton given up by the hydrogen to the oxygen. Energy is produced. The waste product of this process is water. Similar to a battery, each fuel cell stack is electrically connected in series to achieve a higher voltage. Unlike chemical-reaction batteries, fuel cells last as long as the supply of oxygen and hydrogen lasts.

Electric fuel cells are used for a variety of power applications to include: cell phones, cars, bikes, submarines, UAVs, satellites, commercial and residential power production. A Proton Exchange Membrane (PEM) type Ballard Fuel Cells fuel cell was employed successfully in the late 1980's by Canada in a commercial submarine [17]. Congress, within the National Defense Authorization Act for fiscal year 1998, requested DoD to report on the development and application of fuel cells [2]. DoD has established the DoD Fuel Cell Demonstration Program. This program is intended to stimulate growth and economies in the fuel cell industry. DoD also established the Fuel Cell Test and Evaluation Center run by the US Army Corps of Engineers. This center is responsible for validating fuel cell technology.

There have been several initiatives in the last decade to determine the viability of fuel cell usage within the DoD. These include: US Coast Guard test of Molten Carbonate fuel cell technology aboard the CGC Vindicator in 1994 [18]; ONR-sponsored ship impact studies; a 500 Watt sulfur solid oxide fuel cell technology test in 1997 started through a Navy SBIR; and a Marine Corps deployment of light weight Proton Exchange Membrane Technology in exercises in Hawaii in 1999 and 2000 [19]. There are over 50 DoD installations now using fuel cells [2]. Most initiatives have shown favorable results using the fuel cells including indication of lower fueling costs for fixed land sites and increased ranges for vehicles using fuel cells.

THIS PAGE INTENTIONALLY LEFT BLANK

APPENDIX B   DERIVATION OF COUNTER EMF

This Appendix shows the basic derivation of the counter EMF produced by the magnetic fuel cell. The cross-section of core is shown in Figure 27. The equation for magnetic flux density produced from a straight wire of length, L, and direct current, I, is shown by [10]

$$B = \frac{\mu_o \mu_r I L}{4\pi r \sqrt{\left(\frac{L}{2}\right)^2 + r^2}} \, , \tag{4.1}$$

where r is the perpendicular distance from the loop edge to the center of the loop.
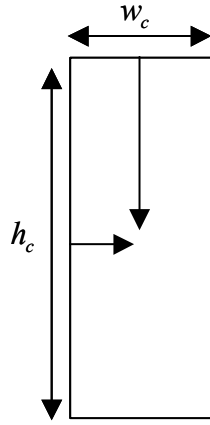
Figure 27   Cross Section of the Soft Magnetic Core.

The magnetic flux density from a rectangular loop is the sum of the magnetic flux densities of the four sides developed using Equation (4.1). Therefore, for side h_c, the magnetic flux density becomes

$$B = \frac{\mu_o \mu_{core} I h_c}{4\pi \frac{w_c}{2} \sqrt{\left(\frac{h_c}{2}\right)^2 + \left(\frac{w_c}{2}\right)^2}} \, . \tag{4.2}$$

The magnetic flux density for side L becomes:

$$B = \frac{\mu_o \mu_{core} I w_c}{4\pi \frac{h_c}{2} \sqrt{\left(\frac{w_c}{2}\right)^2 + \left(\frac{h_c}{2}\right)^2}} .$$ (4.3)

Due to symmetry the magnetic flux density for each parallel wire can be doubled resulting in the flux density at the center of the gap, B_{center}, as Equation (4.4) or re-arranged for current, Equation (4.5),

$$B_{center} = \frac{2\mu_o \mu_{core} I}{\pi} \frac{\sqrt{h_c^2 + w_c^2}}{w_c h_c} ,$$ (4.4)

$$I = \frac{\pi B w_c h_c}{2\mu_o \mu_{core} \sqrt{h_c^2 + w_c^2}} .$$ (4.5)

APPENDIX C: DERIVATION OF THE PREDICTED VALUES

This Appendix determines the predicted output parameters of the magnetic fuel cell experiment using equations derived in Chapter III. Three steps are performed. Step one determines the timing of the magnetic fuel cell. Step two determines the magnetic parameters of the magnetic fuel cell using magnetic circuit analysis. Step three uses the parameters found in the previous two steps to determine the predicted output.

The first step is to determine the initial parameters in the gas chamber (note: actual values and unit have been provided to aid understanding of the development and ease unit analysis):

$$P_s = P_{gap} = 34.5 \text{ MPa}$$

$$m_s = \frac{PV}{RT} M = \frac{(34.5 \text{ MPa})0.37 \text{ m}^3}{\left(8.314 \dfrac{\text{J}}{\text{mol} - \text{K}}\right)293 \text{ K}} \left(0.029 \frac{\text{kg}}{\text{mol}}\right) = 152 \text{ kg}$$

$$\rho_s = \frac{m_s}{V_s} = \frac{152 \text{ kg}}{0.37 \text{ m}^3} = 410.7 \frac{\text{kg}}{\text{m}^3} = \rho_{gap}$$

$$\rho_{atm} = \frac{P_{atm} M}{RT} = \frac{(101325 \text{ Pa})(0.8 \times 0.028 + 0.2 \times 0.032) \dfrac{\text{kg}}{\text{mol}}}{\left(8.314 \dfrac{\text{J}}{\text{mol} - \text{K}}\right)293 \text{ K}} = 1.198 \frac{\text{kg}}{\text{m}^3}$$

$$m_{atm} = \rho_{atm} V_{gap} = \left(1.198 \frac{\text{kg}}{\text{m}^3}\right)1.5 \times 10^{-4} \text{ m}^3 = 1.8 \times 10^{-4} \text{ kg}$$

$$m_{gap} = \rho_{gap} V_{gap} = \left(410.7 \frac{\text{kg}}{\text{m}^3}\right)1.5 \times 10^{-4} \text{ m}^3 = 0.0616 \text{ kg.}$$

The next step is to determine the time for the gas to exit the chamber.

$$v_{valve2} = \sqrt{2\left(\frac{P_{gap}}{\rho_{gap1}} - \frac{P_{atm}}{\rho_{atm}}\right)} = \sqrt{2\left(\left|\frac{34.5 \text{ MPa}}{410.7 \dfrac{\text{kg}}{\text{m}^3}} - \frac{101325 \text{ Pa}}{1.198 \dfrac{\text{kg}}{\text{m}^3}}\right|\right)} = 35 \frac{\text{m}}{\text{s}}$$

$$\dot{m}_{out} = \rho_{gap1} A_{gap1} v_{valve2} = 410.7 \frac{\text{kg}}{\text{m}^3} (0.001171 \text{ m}^2) 35 \frac{\text{m}}{\text{s}} = 16.8 \frac{\text{kg}}{\text{s}} \quad .$$

$$\Delta t_{out} = \frac{m_{gap}}{\dot{m}_{out}} = \frac{0.0616 \text{ kg}}{16.8 \dfrac{\text{kg}}{\text{s}}} = 0.00366 \text{ s}$$

The timing of the fuel cell has been determined; the next series of steps analyzes the magnetic circuit portion of the magnetic fuel cell. This analysis starts off with the determination of the operating point of the magnetic circuit [5].

First the susceptibility, χ, is determined and the permeability, μ, of the experiment,

$$L_{core} \sim \pi w_m = 3.14 \times \frac{0.0508}{2} = 0.08 \text{ m}$$

$$h_c = h_m = 0.2032 \text{ m}$$

$$w_c = w_m = 0.0508 \text{ m}$$

$$\chi_{gap} = -\frac{4\pi\rho_{gap}\kappa_{gap}}{M_{gap}} = -\frac{4\pi\left(410.7 \times 0.2 \frac{\text{kg}}{\text{m}^3}\right)3449 \times 10^{-6} \frac{\text{cm}^3}{\text{mol}}}{0.032 \frac{\text{kg}}{\text{mol}}} 10^{-6} \frac{\text{m}^3}{\text{cm}^3} = 0.000111$$

$$\mu_{gap} = 1 + \chi_{gap} = 1.00011$$

$$\chi_{O_2} = \frac{4\pi\rho_{O_2}\kappa_{O_2}}{M_{O_2}} = \frac{4\pi\left(1.198 \frac{\text{kg}}{\text{m}^3} \times 0.2\right)3449 \times 10^{-6} \frac{\text{cm}^3}{\text{mol}}}{0.032 \frac{\text{kg}}{\text{mol}}} 10^{-6} \frac{\text{m}^3}{\text{cm}^3} = 3.25 \times 10^{-7}$$

$$\mu_{air} = 1 + \chi_{O_2} = 1.0000003245.$$

Next determine the magnetic flux density into the gap, B_{in},

$$H_c = \frac{11600}{0.01257} \frac{\text{A}}{\text{m}} = 922832 \frac{\text{A}}{\text{m}} \quad (conversion)$$

$$k_{loop} = \frac{\pi w_c h_c}{2\mu_{core}\sqrt{h_c^2 + w_c^2}} = \frac{\pi}{2} \frac{(0.0508 \times 0.2032)}{\sqrt{0.2032^2 + 0.0508^2}} = 0.077 \text{ m}$$

$$H_m = \frac{-B_r}{\frac{\mu_o L_m}{\frac{L_{gap}}{\mu_{gap}} + \frac{L_{core}}{\mu_{air}} - k_{loop}} + \frac{B_r}{H_c}}$$

$$H_m = \frac{-1.25\ \text{T}}{\dfrac{4\pi \times 10^{-7} \times 0.0127\ \text{m}}{\dfrac{0.0508\ \text{m}}{1.00011} + \dfrac{0.08\ \text{m}}{1.000000325}} + \dfrac{1.25\ \text{T}}{922832\ \dfrac{\text{A}}{\text{m}}}}$$

$$H_m = -846571\ \frac{\text{A}}{\text{m}}$$

$$B_{in} = \frac{4\pi x 10^{-7} \times 846571\ \dfrac{\text{A}}{\text{m}} \times 0.0127\ \text{m}}{\dfrac{0.0508\ \text{m}}{1.00011} + \dfrac{0.16\ \text{m}}{1.000000361} - 0.077}$$

$$B_{in} = 0.100981\ \text{T}.$$

Second, determine the magnetic flux density as the gas chamber is discharged.

$$\mu_{gap_2} = 1 + \chi_{O_2} = 1.000000325$$

$$H_m = \frac{-B_r}{\dfrac{\mu_o L_m}{\dfrac{L_{gap}}{\mu_{gap}} + \dfrac{L_{core}}{\mu_{air}}} + \dfrac{B_r}{H_c}}$$

$$H_m = \frac{-1.25\ \text{T}}{\dfrac{4\pi \times 10^{-7} \times 0.0127\ \text{m}}{\dfrac{0.0508\ \text{m}}{1.000000345} + \dfrac{0.08\ \text{m}}{1.000000345}} + \dfrac{1.25\ \text{T}}{922832\ \dfrac{\text{A}}{\text{m}}}}$$

$$H_m = -846574\ \frac{A}{m}$$

$$B_{out} = \frac{4\pi \times 10^{-7} \times 846574\ \dfrac{\text{A}}{\text{m}} \times 0.0127\ \text{m}}{\dfrac{0.0508\ \text{m}}{1.000000345} + \dfrac{0.08\ \text{m}}{1.000000345} - .077\ \text{m}}$$

$$B_{out} = 0.100977\ \text{T}$$

$$\Delta B = B_{out} - B_{in} = 4\ \mu\text{T}.$$

Therefore the measured voltage can be calculated, along with the current and inductance [20]:

$$V_{out} = -n \frac{\Delta B}{\Delta t_{in}} A = -515 \times \frac{4 \, \mu T}{0.00366 \, s} \times 0.0102 \, m^2 = -5.5 \, mV$$

$$R_e = \frac{1}{\frac{1}{32 \, \Omega} + \frac{1}{10^7 \, \Omega}} = 31.99 \, \Omega$$

$$V_{measured} = \frac{V_{out} R_e}{R + R_e} = \frac{-5.5 \, mV \times 31.99 \, \Omega}{32 \, \Omega + 31.99 \, \Omega} = -2.75 \, mV$$

$$I = \frac{V_{out} - V_{measured}}{R} = \frac{-5.5 \, mV + 2.75 \, mV}{32 \, \Omega} = -86 \, mA.$$

$$L = \mu_o a \left[\ln\left(\frac{8a}{b}\right) - 1.75 \right] n^2$$

$$L = 4\pi \times 10^{-7} \times 0.05 \left[\ln\left(\frac{8 \times 0.05}{0.0002}\right) - 1.75 \right] \times (515)^2 = 97.5 \, mH$$

APPENDIX D: DERIVED PARAMETERS

Appendix D shows the complete list of input data, constants and derived parameters for the experiment.

Table 2.   Table of Derived Input Values and Constants.

Input Values	Magnitude	Units
Supply Gas Pressure	12,400,000	Pa
Supply Gas Temperature	293	K
Atmospheric Pressure	101,352	Pa
Gap Volume	150	m^3
Width of Magnets	0.0508	m
Height of Magnets	0.2032	m
Length of Magnets (combined)	0.0125	m
Length of Gap	0.0508	m
Coercivity	922,832	A/m
Residual Magnetism	1.25	T
Number of Windings	515	-
Radius of Wire	0.0002	m
Constants		
Ideal gas constant	8.314	J/(mol-K)
Molar Mass of Nitrogen Gas	0.028	kg/mol
Molar Mass of Oxygen Gas	0.032	kg/mol
Experimental Susceptibility of Oxygen	0.0034	cm^3/mol
Permeability of Free Space	0.00000126	H/m

Table 3. Table of Derived Output Values.

Output Parameters	Predicted	Units
Supply Tank Volume (at 1800 psi)	0.37	m3
Molar Mass of Air	0.029	kg/mol
Mass of Gas in Supply Tank	152	kg
Density of Gas in Supply Tank	410.7	kg/m^3
Density of atmosphere	1.198	kg/m^3
Mass of Gas in Gap (at 14.7 psi)	18,000	kg
Mass of Gas in Gap (at 1800 psi)	0.0616	kg
Density of Gas in Gap (at 1800 psi)	410.7	kg/m^3
Pressure of Gap in Gap	12,400,000	Pa
Velocity of the Gas Entering Valve 2	35	m/s
Area Gap Gas	0.001171	m^2
Mass Flow Rate of Gas Out of Gap	16.8	kg/s
Time for Gas to Discharge	0.00366	s
Length of Magnetic Return Path	0.08	m
Height of Magnetic Return Path	0.2032	m
Width of Magnetic Return Path	0.0508	m
Density of Oxygen in Gap (at 1800 psi)	82.14	kg/m^3
Susceptibility of Gap (at 1800 psi)	0.000111	-
Permeability of Gap (at 1800 psi)	1.00011	-
Density of Oxygen (at 14.7 psi)	0.2396	kg/m^3
Susceptibility of Gap (at 14.7 psi)	0.00000033	-
Permeability of Gap (at 14.7 psi)	1.00000032	-
Kloop	0.077	m
Magnetic Field Strength of Magnets (1800 psi)	−846571	A/m
Magnetic Flux Density (1800 psi)	−0.100981	T
Magnetic Field Strength of Magnets (14.7 psi)	−846574	A/m
Magnetic Flux Density (14.7 psi)	−0.100977	T
Change in Magnetic Flux Density	4	uT
Area Gap Magnetic	0.0102	m^2
Voltage Output of Magnetic Fuel Cell	−5.5	mV
Effective Coil Radius	0.05	m
Effective Load Resistance	32.0	ohms
Measured Voltage	−2.75	mV
Current Output of Magnetic Fuel Cell	−86	mA
Inductance of Coil	97.5	mH

APPENDIX E: LIST OF SYMBOLS

H_c	coercivity
χ	susceptibility
μ_r	relative permeability
B	magnetic flux density
H	magnetic field strength
μ_o	permeability of free space
κ	experimental susceptibility
M	molar mass
ρ	material density
M	magnetization
μ	magnetic permeability
N_v	number of atoms per unit volume
q	electron charge
$<r^2>$	expectation value of orbital area
Z	atomic number
m_e	electron mass
N_2	nitrogen
Br_2	bromine
Bi	bismuth
O_2	oxygen
μ_m	atomic magnetic moment

K_B	Boltzmann constant
T	temperature
$\mathfrak{I}$	magneto-motive force
$d\vec{L}$	unit length
n	number of windings
I	induced current
H_c	core magnetic field strength
L_c	mean length of core
H_g	gap magnetic field strength
L_g	gap length
A	cross-sectional area of magnetic material
ϕ	magnetic flux
$\mathfrak{R}$	reluctance
V	voltage
R	resistance
ΔE_{KE}	change in kinetic energy of gas
ΔE_{PE}	change in potential energy of gas
ΔE_{gas}	change in pressure energy of gas
v_f	final velocity of gas
v_i	initial velocity of gas
g	gravity
h_f	final height of gas
m	mass of the gas

h_i	initial height of gas
V_g	gas volume
P_f	final pressure of gas
P_i	initial pressure of gas
v	gas velocity
ΔP	change in pressure of gas
n_m	number of moles
R	gas constant
γ	ideal gas constant
$\Delta\phi$	flux change
Δt	change in time
ΔB	change in magnetic flux density
χ_f	final susceptibility
χ_i	initial susceptibility
$\Delta\chi$	change in susceptibility
H_f	final magnetic field strength
H_i	initial magnetic field strength
h	height of gap
v_{valve1}	velocity of gas entering valve one
v_s	velocity of the gas in the supply tank
P_s	pressure of the gas in the supply tank
ρ_s	density of gas in the supply tank

P_{gap}	pressure of the gas in the gap
ρ_{gap}	density of the gas in the gap
A_{valve1}	cross-sectional area of the supply valve
A_{gap}	cross-sectional area of the gap
v_{valve1}	velocity of the gas entering valve one
v_{gap-in}	velocity of the gas entering the gap
h_{gap}	height of the gap
v_{valve2}	velocity of the gas exiting valve two
$v_{gap-out}$	velocity of the gas leaving the gap
P_{atm}	atmospheric pressure
ρ_{atm}	atmospheric density
A_{valve2}	cross-sectional area of valve two
v_{atm}	velocity of the gas entering the atmosphere
t_{cycle}	cycle time of the magnetic fuel cell
t_{valve1}	time to open and shut valve one
t_{valve2}	time to open and shut valve two
f_{cycle}	cycle frequency of the magnetic fuel cell
$\dot{V}_{cycle}$	volume flow rate of the cycle
t_d	duration time
J	induced current density
ds	unit area normal to the magnetic flux

H_m	magnet magnetic field strength
L_m	length of magnets
H_{gap}	gap magnetic field strength
L_{gap}	length of the gap
H_{core}	core magnetic field strength
L_{core}	length of the core
B_{gap}	gap magnetic flux density
B_{core}	core magnetic flux density
B_m	magnet magnetic flux density
μ_{gap}	gap permeability
μ_{core}	core permeability
k	simplification constant
h_c	core height
w_c	core width
B_r	residual magnetization
μ_m	permeability of magnets
H_c	magnet coercivity
B_{in}	magnetic flux density at high pressure
B_{out}	magnetic flux density at atm. pressure
ΔE_{cycle}	electrical energy of the cycle
R	load resistance

P_{cell}	power output of the magnetic fuel cell each cycle
ΔP_{mag}	magnetic pressure drop caused by magnetic fuel cell
ε	efficiency of the magnetic fuel cell
ΔE_{total}	total energy of the gas
ΔE_{cell}	total energy of the magnetic fuel cell
$\dfrac{n^2}{R}$	power factor term
x	horizontal distance
y	vertical distance
a	magnetic core radius
b	wire radius
n_{layer}	number of windings on a layer
n_y	total number of layers
$L_{layer\,1}$	length of first layer
$L_{layer\,2}$	length of second layer
L_{coil}	total length of coil
ρ_w	resistivity of wire
A_{wire}	cross-sectional area of wire
$I(t)$	output current with respect to time
I_o	initial current at time zero
R_e	effective resistance of the circuit
L	inductance of the test coil

t	time
C	capacitance of the magnetic fuel cell coil
f	resonant frequency of calibration circuit
I_{pk-1}	output current at peak one
V_{pk-1}	output voltage at peak one
I_{pk-2}	output current of next peak
V_{pk-2}	output voltage of next peak
Δt_{peaks}	time difference between peaks
A_{test}	area of test coil
$A_{chamber}$	area of pressure chamber
A_m	fuel cell magnetic cross-section area
k_c	coupling factor
V_{out}	voltage output of fuel cell
r	perpendicular distance from loop edge to center of loop
B_{center}	flux density at the center of gap

THIS PAGE INTENTIONALLY LEFT BLANK

LIST OF REFERENCES

1. Reese, R. L., *University Physics*, Brooks/Cole Publishing Company, Pacific Grove, 2000.

2. Department of Defense, "Report to Congressional Defense Committees on the Utilization and Demonstration of Fuel Cells," DoD Fuel Cell, http://www.dodfuelcell.com/lib_resources.html, pp. 1-38, 1998.

3. Davidson, P. A., *An Introduction to Magnetohydrodynamics*, Cambridge University Press, Cambridge, 2001.

4. Simon, M. D., Heflinger, L. O., Geim, A. K., "Diamagnetically stabilized magnet levitation." *American Journal of Physics*, Vol. 69, No. 6, pp. 702-713, 2001.

5. Furlani, E. P., *Permanent Magnet and Electromechanical Devices Materials, Analysis, and Applications*, Academic Press, San Diego, 2001.

6. Lide, D. R., *CRC Handbook of Chemistry and Physics*, CRC Press, New York, 83rd Edition, 1999.

7. Kittel, C, *Introduction to Solid State Physics*, John Wiley & Sons, Inc., New York. 1996.

8. Huang, K, *Statistical Mechanics*, John Wiley & Sons, New York, 1987.

9. Young, Hugh D., *University Physics*, 8th Ed., Addison-Wesley, 1992.

10. Cheng, D. K., "Static Magnetic Fields," in *Field and Wave Electromagnetics*, pp. 225-512, Addison-Wesley Publishing Company, Menlo Park, CA, 1989.

11. Sunnyvale Valve and Fitting, *The SWAGELOK Companies Product Guide*, 929 Weddell Court, Sunnyvale, CA, 94089, 1991.

12. Stanford Magnetics, 4 Meadowpoint, Aliso Viejo, CA 92656, U.S.A.

13. COMSOL, Inc., 8 New England Executive Park, Suite 310, Burlington, MA 01803.

14. Uetake, Hiromichi; Nakagawa, Jun; Horota, Noriyuka; and Kitazawa, Koichi; "Nonmechanical magnetothermal wind blower by a superconductor," *Journal of Applied Physics*, Vol. 85, No. 8, pp. 5735-5737, 1999.

15. Feynman, R, Leighton, R., and Sands, M., "Chapter 9: Electricity in the Atmosphere." in *The Feynman Lectures on Physics*. Volume 2. Reading, MA: Addison-Wesley Publishing Company, Inc.. 1966.

16. Prohaska, Don, "The Birth of the Fuel Cell – But Who is the Father?", *European Fuel Cell Forum*, 13 August, 2001, http://www.efcf.com/media/ep010813.shtml, Accessed 01 December 2001.

17. Ballard Power Systems, 9000 Glenlyon Parkway, Burnaby, BC V5J 5J9 Canada, http://www.ballard.com/.

18. Allen, S., Asheye, E., Gore, D., Woerner, J., Cervi, M., "Marine Applications for Fuel Cells," *Naval Engineers Journal*, pp. 93-106, January 1998.

19. Ball Aerospace, "Fuel Cells Newsletter," Ball Aerospace, http://www.ball.com/aerospace/pdf/pps_1q_news.pdf, Boulder, Colorado, pp. 1-6, 2000.

20. Knoepfel, E. Heinz, *Magnetic Fields, A Comprehensive Theoretical Treatise for Practical Use*, John Wiley & Sons, New York, 2000.

INITIAL DISTRIBUTION LIST

1.   Defense Technical Information Center
   Ft. Belvoir, VA

2.   Dudley Knox Library
   Naval Postgraduate School
   Monterey, CA

3.   Dr. Todd Weatherford, Code EC
   Department of Electrical and Computer Engineering
   Naval Postgraduate School
   Monterey, CA

4.   Dr. Gamani Karunasiri, Code PH
   Department of Physics
   Naval Postgraduate School
   Monterey, CA

5.   Dr. John Powers (Chairman), Code EC
   Department of Electrical and Computer Engineering
   Naval Postgraduate School
   Monterey, CA

6.   Dr. James Luscombe, Code PH
   Department of Physics
   Naval Postgraduate School
   Monterey, CA

7.   Dr. Christopher Brophy, Code AA
   Department of Aerospace
   Naval Postgraduate School
   Monterey, CA

8.   Don Lincoln, Code 006
   Patent Attorney
   Naval Postgraduate School
   Monterey, CA

9.   Dr. Sherif Michael, Code EC
   Department of Electrical and Computer Engineering
   Naval Postgraduate School
   Monterey, CA

10. Dr. Bruce Denardo, Code PH
    Department of Physics
    Naval Postgraduate School
    Monterey, CA

11. Dr. Michael Morgan, Code EC
    Department of Electrical and Computer Engineering
    Naval Postgraduate School
    Monterey, CA

12. Dr. Jovan Lebaric, Code EC
    Department of Electrical and Computer Engineering
    Naval Postgraduate School
    Monterey, CA

13. Dr. Dave Jenn, Code EC
    Department of Electrical and Computer Engineering
    Naval Postgraduate School
    Monterey, CA

14. Dr. Richard Adler, Code EC
    Department of Electrical and Computer Engineering
    Naval Postgraduate School
    Monterey, CA

15. Research Assistant Andrew Parker, Code EC
    Department of Electrical and Computer Engineering
    Naval Postgraduate School
    Monterey, CA

16. Lab Tech Mitch Little, Code EC
    Department of Electrical and Computer Engineering
    Naval Postgraduate School
    Monterey, CA

17. Electronics Lab Technician Jeff Knight, Code EC
    Department of Electrical and Computer Engineering
    Naval Postgraduate School
    Monterey, CA

18. Lab Director Don Snyder, Code EC
    Department of Electrical and Computer Engineering
    Naval Postgraduate School
    Monterey, CA

19.   Lab Tech Michael Myshka, Code EC
        Department of Electrical and Computer Engineering
        Naval Postgraduate School
        Monterey, CA

20.   LCDR Joe Brennan
        PSC 276 Box 265
        APO AP 96548

21.   Dr. Robert Nowack
        Defense Advanced Research Projects Agency
        Arlington, VA

22.   Dr. Richard Carlin
        Office of Naval Research
        Arlington, VA

23.   Stephen Bloor
        Patent Attorney
        National Security Agency
        Fort Meade, MD